NASA Technical Memorandum 86314

Exploratory Investigation of the Aerodynamic Characteristics of a Biwing Vehicle at Mach 20.3

Peter T. Bernot

FEBRUARY 1985

NASA

NASA Technical Memorandum 86314

Exploratory Investigation of the Aerodynamic Characteristics of a Biwing Vehicle at Mach 20.3

Peter T. Bernot
Langley Research Center
Hampton, Virginia

NASA
National Aeronautics
and Space Administration
Scientific and Technical Information Branch
1985

Summary

Aerodynamic characteristics of a simple biwing configuration have been obtained at Mach 20.3 at a Reynolds number of 3.2×10^6, based on body length. The body consisted of a cylindrical section and an ogival nose having an overall fineness ratio of 6.67. The delta wings were geometrically similar with the upper wing located slightly forward relative to the lower wing. Longitudinal and lateral-directional data were obtained over an angle-of-attack range from $-3°$ to $50°$ with the model oriented in the upright and inverted positions.

With the center of gravity at 75 percent of body length, the upright version had a stable trim point at 17° angle of attack, whereas the inverted version trimmed at 15°. As angle of attack increased to 50°, both versions exhibited pitch-up characteristics, especially the inverted version. The inverted model yielded the higher value of maximum lift-drag ratio L/D of 1.44 at 20° angle of attack. The upright model produced a maximum value of L/D value of 1.32 that occurred at angles of attack from about 20° to 26°.

Both the upright and inverted versions of the model were directionally unstable over the entire test angle-of-attack range. The upright version was more unstable, mainly because of a lower value of the side-force derivative C_{Y_β}. In general, both versions had positive effective dihedral at positive angles of attack.

Introduction

For the past several years, the National Aeronautics and Space Administration (NASA) and industry have been studying advanced Earth-to-orbit transportation systems that incorporate improved state-of-the-art technologies. Most of the various configurations under study had delta wings and large vertical tails that were later modified by reducing the wing size, removing the vertical tail, and adding small wing-tip fins. Many aspects of these concepts are discussed in references 1 to 4.

Since these concepts have the center of gravity far aft and are difficult to control aerodynamically, other nonconventional configurations have been examined in an attempt to alleviate this problem. An exploratory investigation was initiated on a simple biwing model to determine its aerodynamic characteristics over a wide range of angle of attack at hypersonic speeds. The fuselage consisted of a cylindrical section with an ogival forebody having an overall fineness ratio of 6.67. The cropped delta wings were geometrically similar, having leading-edge sweep angles of 38.3° and the same spans. The upper wing was positioned slightly ahead of the lower wing by a distance equal to 5 percent of the fuselage length.

The purpose of this paper is to present the stability and performance results on this concept at Mach 20.3. Static longitudinal and lateral-directional characteristics were obtained over an angle-of-attack range from $-3°$ to $50°$ at angles of sideslip of $0°$ and $5°$. In order to determine the effects of mutual interference, the biwing model was tested in the upright and inverted orientations. Component breakdown tests were also made for both orientations. This investigation was conducted in the 22-inch aerodynamics leg of the Langley Hypersonic Helium Tunnel Facility.

Symbols

The longitudinal characteristics are based on both the body and stability axis systems. The lateral-directional characteristics are based on the body axis system only. Measurements were made in U.S. Customary Units.

b	reference wing span
C_A	adjusted axial-force coefficient, $\frac{\text{Axial force}}{qS}$
$C_{A,B}$	base pressure coefficient, $\frac{-(p_B - p_\infty)S_B}{qS}$
C_D	drag coefficient, $\frac{\text{Drag force}}{qS}$
C_L	lift coefficient, $\frac{\text{Lift force}}{qS}$
C_l	rolling-moment coefficient, $\frac{\text{Rolling moment}}{qSb}$
C_{l_β}	effective dihedral parameter, $\left(\frac{\Delta C_l}{\Delta \beta}\right)_{\beta=0°,5°}$, per degree
C_m	pitching-moment coefficient, $\frac{\text{Pitching moment}}{qSl}$
C_N	normal-force coefficient, $\frac{\text{Normal force}}{qS}$
C_n	yawing-moment coefficient, $\frac{\text{Yawing moment}}{qSb}$
C_{n_β}	directional stability parameter, $\left(\frac{\Delta C_n}{\Delta \beta}\right)_{\beta=0°,5°}$, per degree
C_Y	side-force coefficient, $\frac{\text{Side force}}{qS}$
C_{Y_β}	rate of change of side-force coefficient with sideslip angle, $\left(\frac{\Delta C_Y}{\Delta \beta}\right)_{\beta=0°,5°}$, per degree
L/D	lift-drag ratio
l	fuselage reference length
M	free-stream Mach number
p	pressure
q	free-stream dynamic pressure
R_l	Reynolds number based on fuselage length
S	wing reference area

S_B fuselage base area

x_{cp}/l location of center of pressure measured from nose of fuselage

α angle of attack, deg

β angle of sideslip, deg

Subscripts:

∞ free-stream conditions

$0.75l$ 75 percent of fuselage length

Model-component designations:

B body or fuselage

W_L lower wing with model in upright position

W_U upper wing with model in upright position

Description of Model

The body was comprised of a cylinder 4.85 in. long with a 1.15-in-long ogival nose having an overall fineness ratio of 6.67. Both wings were geometrically similar in that each had the same leading-edge sweep, span, and aspect ratio. The reference area S was based on the total planform area of the upper wing (W_U). It should be noted that the upper wing was located ahead of the lower wing by 0.3 in. The wing airfoil sections were NACA 0008-64 at the root and NACA 0012-64 at the tips. A sketch of the model is presented in figure 1, and photographs of the test model are presented in figure 2.

Apparatus and Tests

Wind Tunnel

This investigation was conducted in the 22-inch aerodynamics leg of the Langley Hypersonic Helium Tunnel Facility. This facility has a contoured axisymmetric nozzle with circular cross sections and a nominal test-section Mach number of 20. Calibration surveys of reference 5 indicate a range of Mach number from 17.6 to 22.2 at stagnation pressures from 200 to 3000 psia, respectively. The tunnel is usually operated at stagnation temperatures near ambient. If desired, the stagnation temperature may be varied up to about 500°F by use of an electrical resistance heater. This facility operates in the blowdown mode in which the average test run is about 30 sec. After each run, the helium is reclaimed, purified, and stored in high-pressure tanks for use in subsequent tests.

Tests

All tests were conducted at a stagnation pressure of 1000 psia at a temperature of about 60°F. The free-stream Mach number was 20.3 at a Reynolds number of 3.2×10^6, based on model body length. The free-stream flow properties were corrected for real-gas effects by the methods of reference 6.

Force and moment data were obtained over an angle-of-attack range from −3° to 50° by utilizing two sting and balance arrangements. Tests at angles of attack below 19° were made with a straight sting. At higher angles of attack, a 30° prebent sting was used with a different balance designed for higher loads. Data were obtained at the selected angles of attack by using a prism that was flush mounted in the model fuselage, which reflected light from a point source onto electric eyes that were aligned at the selected angles. Details of this system can be found in reference 5. Lateral-directional data were generated by utilizing offset stings having a fixed sideslip angle of about 5°. All moment data were based to the moment center located at the 75-percent body-length station.

The estimated uncertainties of the measured coefficients are based on ±0.5 percent of the design loads for each balance and are presented in the following table:

Coefficient	Low α	High α
C_N	±0.0096	±0.029
C_A	±.0032	±.004
C_m	±.0021	±.004
C_l	±.0009	±.0027
C_n	±.0009	±.0027
C_Y	±.0032	±.0096

The accuracy of the angles of attack and sideslip was estimated to be within ±0.1°, and the accuracy of the free-stream Mach number was estimated to be within ±0.2. Base pressures were measured at one location for all tests. Accordingly, values of axial-force coefficients C_A were adjusted to correspond to a base pressure equal to the free-stream static pressure.

To provide some insight on the complex flow characteristics anticipated for the biwing model, two flow-visualization techniques were utilized. One technique employed an electron-beam device that illuminated the flow field about the model. By photographing the flow field, the various shock systems generated by the model and its components were easily discernible. Details on this flow technique are given in reference 7. The second technique involved obtaining surface oil-flow patterns by using a mixture of lampblack and silicone oil that was applied to the lightpainted model. Prior to the wind-tunnel test, the model was set at the desired angle of attack. Generally, several photographs of the flow patterns existing on the model surfaces were taken after each test run.

Results and Discussion

Longitudinal Characteristics

Complete configuration. The longitudinal characteristics of the complete configuration in the upright and inverted positions are presented in figure 3 over the angle-of-attack range from $-3°$ to $50°$. With the center of gravity at 75 percent of fuselage length, the upright version trimmed at 17° angle of attack, whereas the inverted version had a stable trim point near 15° angle of attack. (See fig. 3(d).) Both versions exhibited pitch-up as angle of attack was increased. For the upright version, pitch-up began to occur at an angle of attack of about 40°. The inverted version had a more severe pitch-up characteristic, which began to occur at about 25° angle of attack. This trend for the latter model was probably due to the forward location of the lower wing, which shielded the upper wing from the flow as angle of attack increased to 50°. As expected, lower values of C_N were obtained again for the inverted version when compared with the upright version as angle of attack was increased from 30° to 50° because of shielding, as shown in figure 3(b). However, the inverted model had higher values of C_N at angles of attack below 30°. This trend may have been caused, in part, by mutual interference effects because of the relative wing locations. In general, the same overall trends of C_N are also reflected for C_L and C_D, as shown in figures 3(e) and 3(f), respectively.

The inverted version exhibits a significant increase in C_A at angles of attack greater than 23°. (See fig. 3(c).) This effect may be due, in part, to the forward lower wing (BW_U) on which the pressure loadings can be relatively higher than those experienced for the upright version. The lower wing is obviously closer to the body bow shock because of its more forward location.

The inverted model had a maximum L/D value of 1.44 that peaked at 20° angle of attack. For the upright model, the maximum L/D was 1.32 and occurred at angles of attack from about 20° to 26°.

Component buildup. The effects of component buildup on the longitudinal characteristics for both upright and inverted versions are presented in figure 4. A configuration description is given in the following table:

Model	Position	Configuration
BW_U	Upright	Flat top
	Inverted	Flat bottom
BW_L	Upright	Flat bottom
	Inverted	Flat top

Consistently higher values of C_N and C_L are obtained for the low-wing or flat-bottom versions (BW_L upright and BW_U inverted) than for the flat-top models, as presented in figures 4(b) and 4(e), respectively. This result is also true for C_A in that the C_A values are significantly higher as angle of attack increases to 50°. This effect for the flat-bottom versions is due to the wing being closer to the body bow shock. From figure 4(c), it is also noted that the more forward flat-bottom model BW_U yields the highest C_A values at angles of attack greater than about 20°. In figure 4(f), values of C_D are consistently greater for these flat-bottom models at positive angles of attack. As shown in figure 4(g), the flat-bottom and flat-top models yielded the same value of maximum L/D, which was about 1.28. This occurs at about 20° angle of attack for the flat-bottom models and near 26° for the flat-top versions. As shown, the body alone has a maximum L/D of 1.16, also occurring at 26° angle of attack. Of the four body-wing configurations tested, the upright flat-bottom version (BW_L) yielded the largest negative increments in C_m when compared to the body-alone model. (See fig. 4(d).) The inverted flat-bottom model (BW_U) also had fairly large negative increments in pitching moment; however, the flat-top model (BW_L inverted) produced slightly greater increments, but only at angles of attack exceeding 40°. This result was mainly due to the rearward wing location causing a rearward movement of the center of pressure as angle of attack increased to 50°.

Lateral-Directional Characteristics

Complete configuration. The lateral-directional characteristics of the complete configuration are presented in figure 5 for both the upright and inverted positions. Both versions are directionally unstable over the entire test angle-of-attack range. The upright version is more unstable than the inverted version because the side-force derivative C_{Y_β} is smaller. At positive angles of attack, both versions have positive effective dihedral $-C_{l_\beta}$. The unusual variations of both curves occurring at the higher angles of attack are probably due to mutual interference effects, especially for the upright version.

Component buildup. The sideslip characteristics for the component buildup configurations are presented in figure 6 at an angle-of-attack range from 20° to 50° for both upright and inverted positions. The four upright configurations shown in figure 6(a) are directionally unstable because of the rearward location of the center of gravity. The flat-top model (BW_U upright) is seen to have the lowest level of instability, resulting from the higher magnitude of the side-force derivative C_{Y_β}. In general, the body alone and the complete model

are more unstable because of the smaller values of C_{Y_β} occurring at angles of attack from 28° to 50°. Consequently, the magnitudes of C_{Y_β} are inversely related to the directional stability levels. With the exception of the body alone, positive dihedral effect $-C_{l_\beta}$ is obtained for the other three configurations. Comparisons of the curves for these models reaffirm the strong influence of mutual interference on C_{l_β} mentioned previously for the complete configuration.

For the inverted position presented in figure 6(b), the four configurations are again directionally unstable. The complete model is seen to have less instability than the flat-top model (BW_L) at angles of attack from 20° to 42°. In this case, mutual interference effects for the complete model can be deemed favorable. The flat-bottom model (BW_U) has the highest level of instability because of the forward location of the wing, which results in reducing the side-force derivative.

The magnitudes of C_{Y_β} for these inverted models are directly related to the levels of directional instability in the same manner as those for the upright models. Positive dihedral effects are again obtained for all three wing configurations. The flat-top model (BW_L inverted) yielded larger values of C_{l_β} when compared with the flat-bottom model.

Flow Visualization

Oil-flow patterns on the upright version of the complete model are presented in figures 7 and 8 for angles of attack of 30°, 40°, and 50°. In figure 7, the complex nature of the flow patterns that exist between the wings is quite apparent at these angles of attack. The influence of the bow shock generated by the upper wing is clearly shown. A vortex is also noted at the junction of the upper wing and body. The magnitude of this vortex system becomes larger as angle of attack increases from 30° to 50°. In figure 8, the flow patterns on the bottom surfaces of the body and both wings are shown for angles of attack of 30°, 40°, and 50°. The stagnation regions on the bottom of the body are clearly seen at these angles of attack. The flow patterns on the bottom surface of the lower wing are unaffected by any flow or shock systems emanating from the upper wing. However, the bottom of the upper wing is strongly affected by the impingement of the leading-edge shock on the lower wing at 30° and 40° angles of attack; the impingement line is clearly shown along the wing span. As angle of attack is increased to 50°, the impingement line moves forward, which probably results in changes on the pressure loadings on the upper wing. In addition, it must be remembered that a vortex system exists on the inboard section of the upper wing at these angles of attack previously shown in figure 7.

In figure 9, photographs of electron-beam illuminated flow fields on the upright model are presented for angles of attack of 20°, 30°, 40°, and 50°. The major item of interest is the relative movement of the leading-edge shock generated by the lower wing as angle of attack increases. This shock system is seen to impinge on the bottom surface of the upper wing where the impingement line moves forward with increasing angle of attack. At 50° angle of attack, this shock system moves slightly ahead of the upper wing. Consequently, the impingement line is not discernible from the oil-flow patterns presented in figure 8.

Concluding Remarks

Aerodynamic characteristics of a simple biwing configuration have been obtained at Mach 20.3 at a Reynolds number of 3.2×10^6, based on body length. The body consisted of a cylindrical section and an ogival nose having an overall fineness ratio of 6.67. The delta wings were geometrically similar with the upper wing located slightly forward relative to the lower wing. Longitudinal and lateral-directional data were obtained over an angle-of-attack range from −3° to 50° with the model oriented in the upright and inverted positions.

With the center of gravity at 75 percent of body length, the upright version had a stable trim point at 17° angle of attack, whereas the inverted version trimmed at 15°. As angle of attack increased to 50°, both versions exhibited significant pitch-up characteristics, especially the inverted version. The inverted model yielded the higher value of maximum lift-drag ratio L/D of 1.44 at 20° angle of attack. The upright model produced a maximum value of L/D of 1.32 that occurred at angles of attack from about 20° to 26°.

Both the upright and inverted versions of the model were directionally unstable over the entire test angle-of-attack range. The upright version was more unstable, mainly because of a lower value of the side-force derivative C_{Y_β}. In general, both versions had positive effective dihedral at positive angles of attack.

Photographs of oil-flow patterns on the upright version of the complete model were made for angles of attack of 30°, 40°, and 50° and show the complex nature of the flow that exists between the wings.

Langley Research Center
National Aeronautics and Space Administration
Hampton, VA 23665
October 24, 1984

References

1. Henry, Beverly Z.; and Decker, John P.: Future Earth Orbit Transportation Systems/Technology Implications. *Astronaut. & Aeronaut.*, vol. 14, no. 9, Sept. 1976, pp. 18–28.

2. Haefeli, Rudolph C.; Littler, Ernest G.; Hurley, John B.; and Winter, Martin G.: *Technology Requirements for Advanced Earth-Orbital Transportation Systems—Final Report.* NASA CR-2866, 1977.
3. Freeman, Delma C., Jr.; and Wilhite, Alan W.: *Effects of Relaxed Static Longitudinal Stability on a Single-Stage-To-Orbit Vehicle Design.* NASA TP-1594, 1979.
4. Bernot, Peter T.: *Effect of Modifications on Aerodynamic Characteristics of a Single-Stage-To-Orbit Vehicle at Mach 5.9.* NASA TM-84565, 1983.
5. Arrington, James P.; Joiner, Roy C., Jr.; and Henderson, Arthur, Jr.: *Longitudinal Characteristics of Several Configurations at Hypersonic Mach Numbers in Conical and Contoured Nozzles.* NASA TN D-2489, 1964.
6. Erickson, Wayne D.: *Real-Gas Correction Factors for Hypersonic Flow Parameters in Helium.* NASA TN D-462, 1960.
7. Weinstein, Leonard M.; Wagner, Richard D., Jr.; Henderson, Arthur, Jr.; and Ocheltree, Stewart L.: *Electron Beam Flow Visualization in Hypersonic Helium Flow.* ICIASF '69 Record, IEEE Publ. 69-C-19 AES, pp. 72–78.

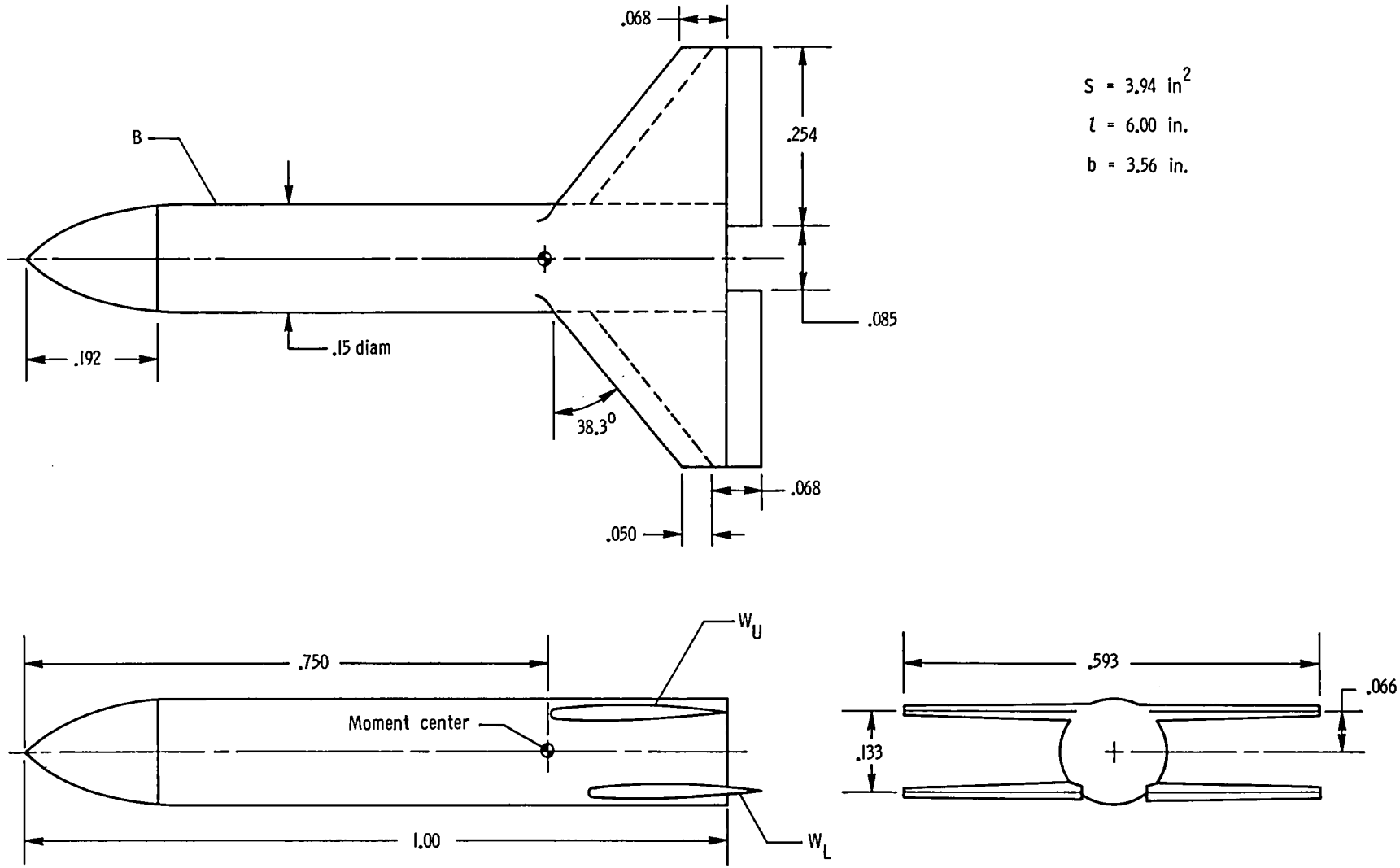

Figure 1. Sketch of model. All dimensions are normalized by model length l.

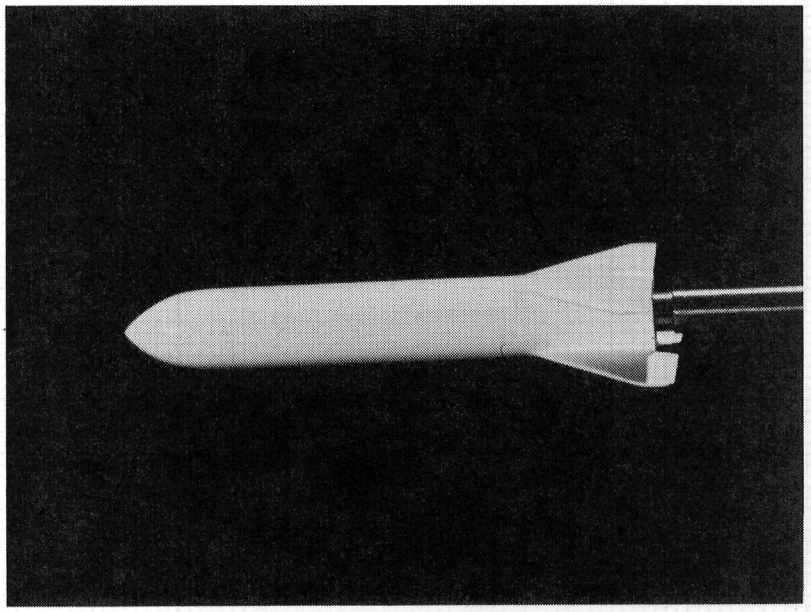

Upright position

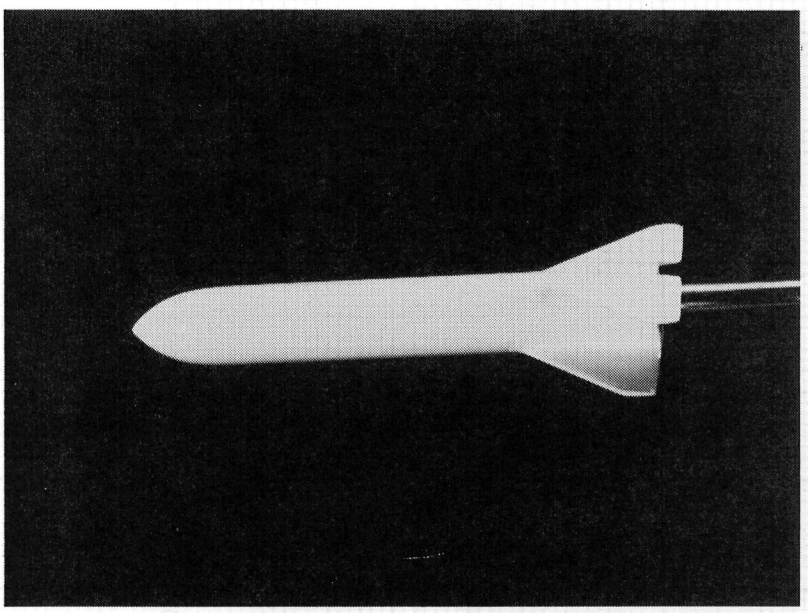

Inverted position

L-84-10,694

Figure 2. Photographs of complete model.

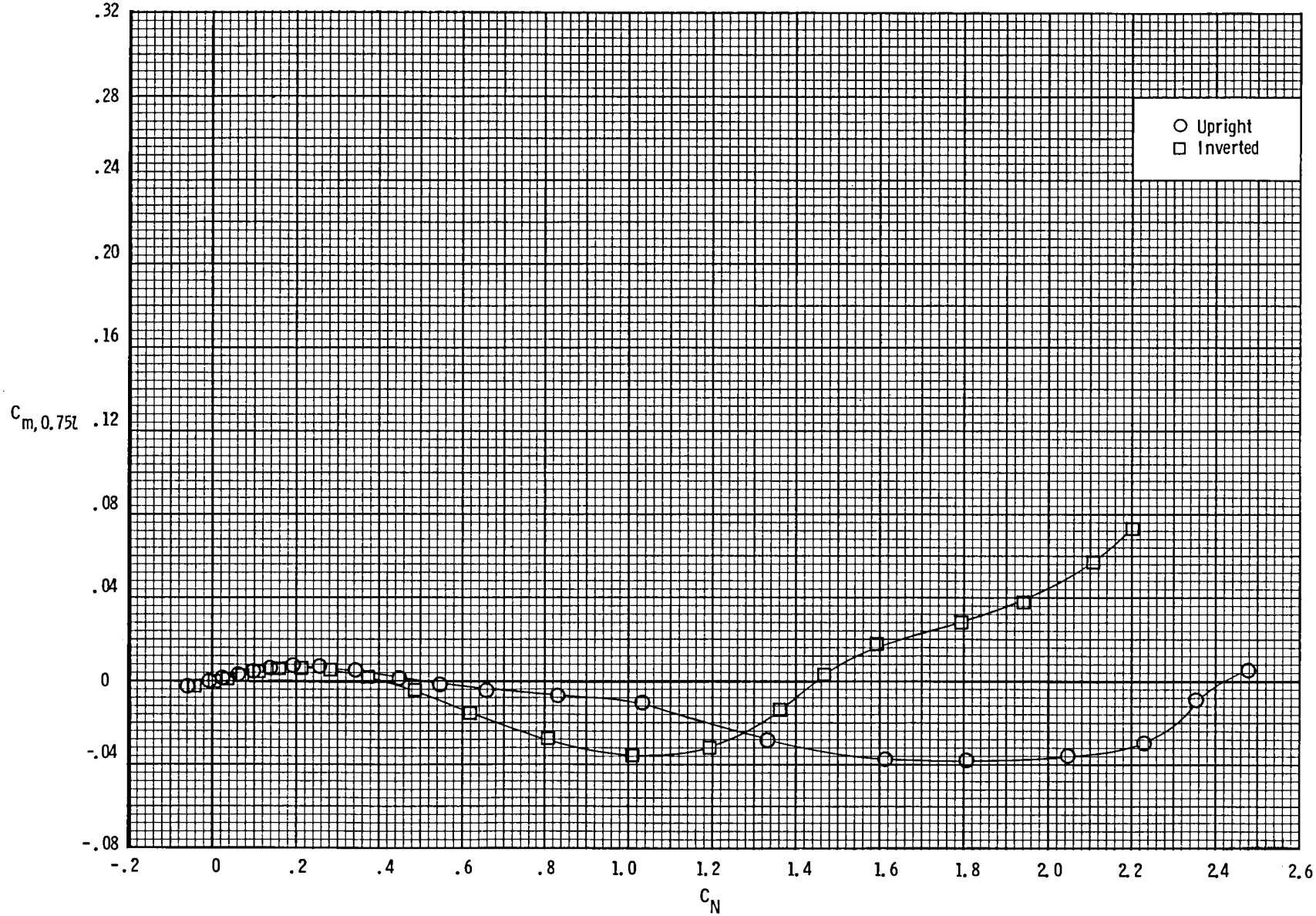

(a) $C_{m,0.75l}$ plotted against C_N.

Figure 3. Longitudinal characteristics of complete configuration in upright and inverted positions. $M = 20.3$; $R_l = 3.2 \times 10^6$.

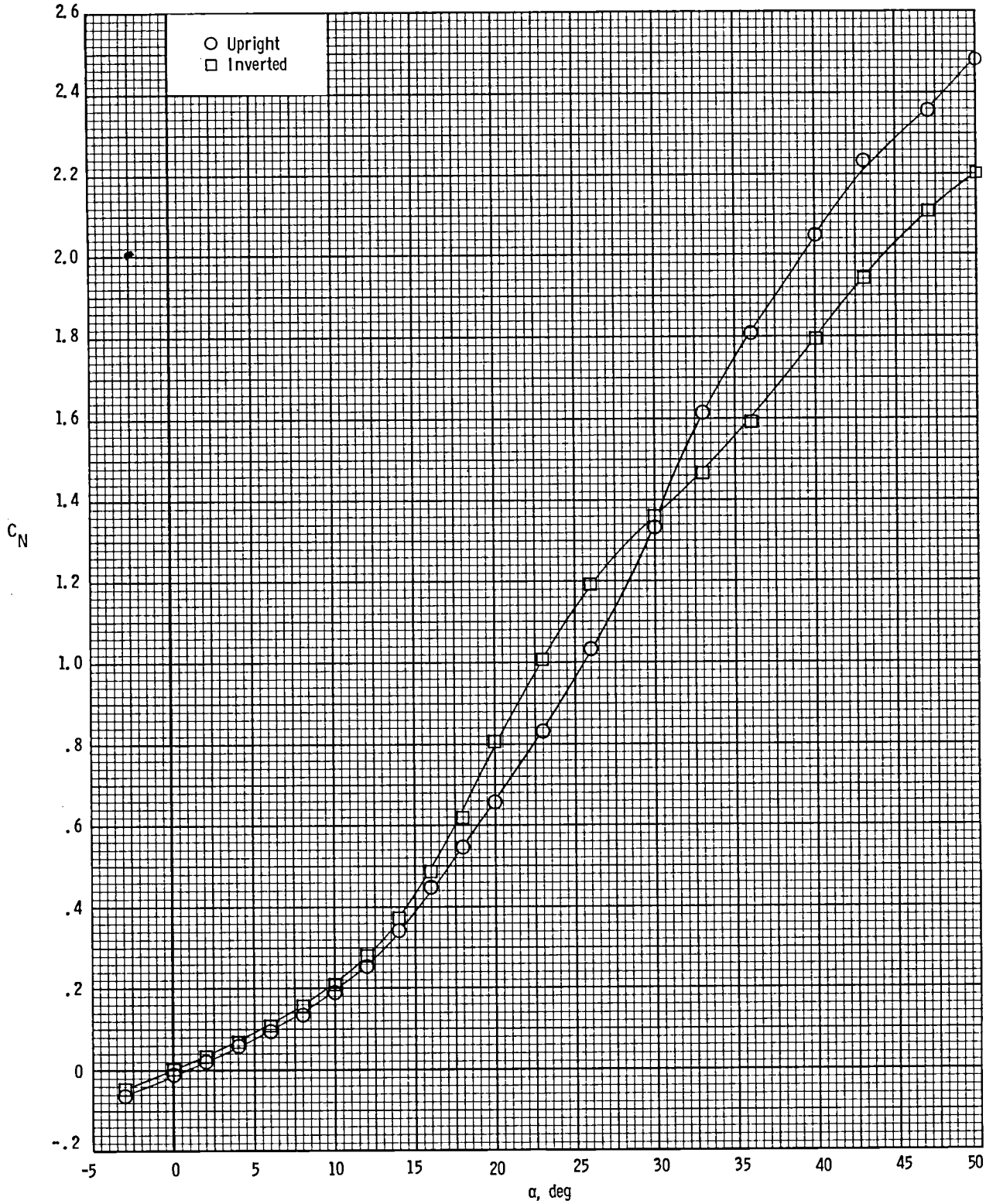

(b) C_N plotted against α.

Figure 3. Continued.

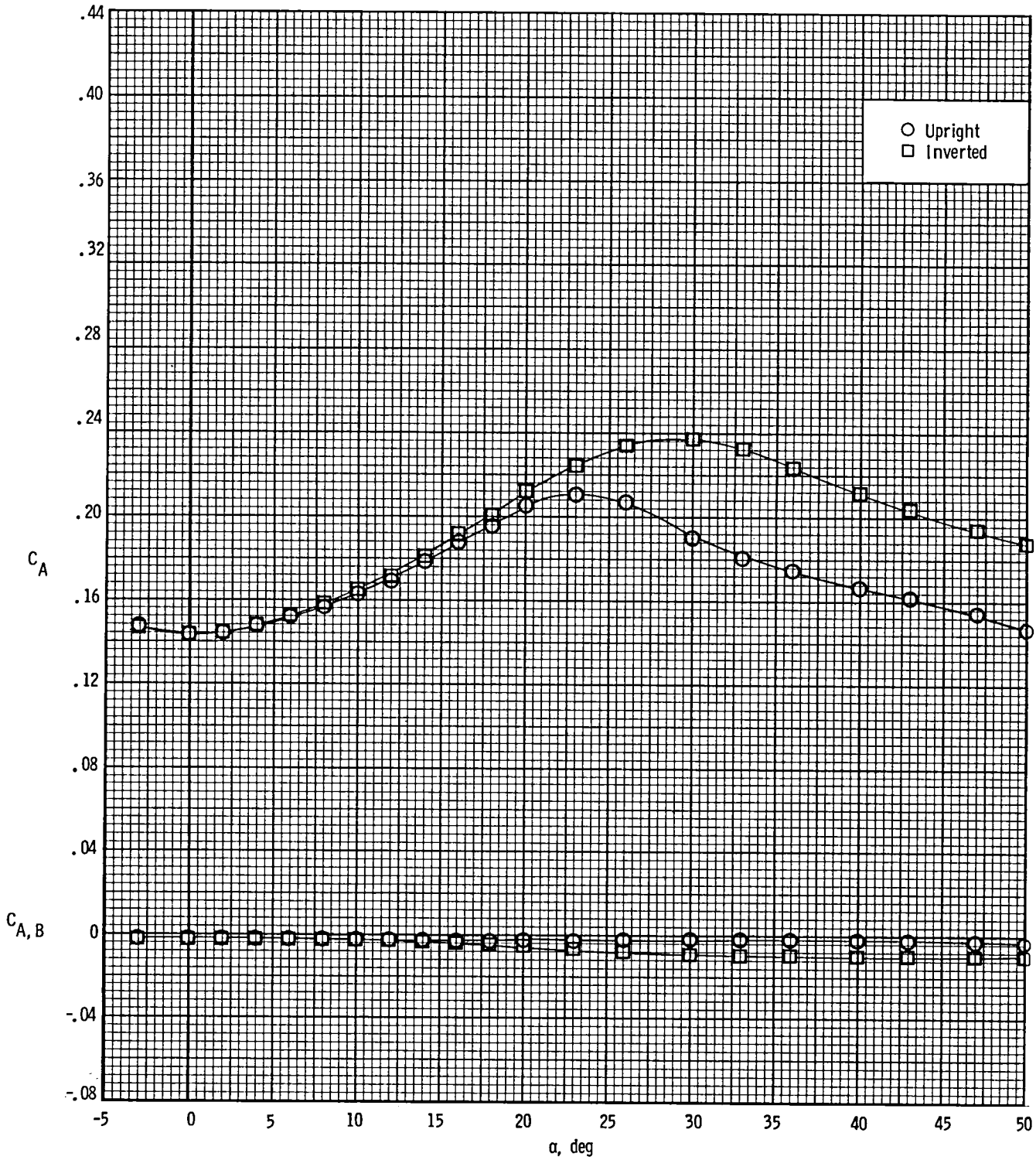

(c) C_A and $C_{A,B}$ plotted against α.

Figure 3. Continued.

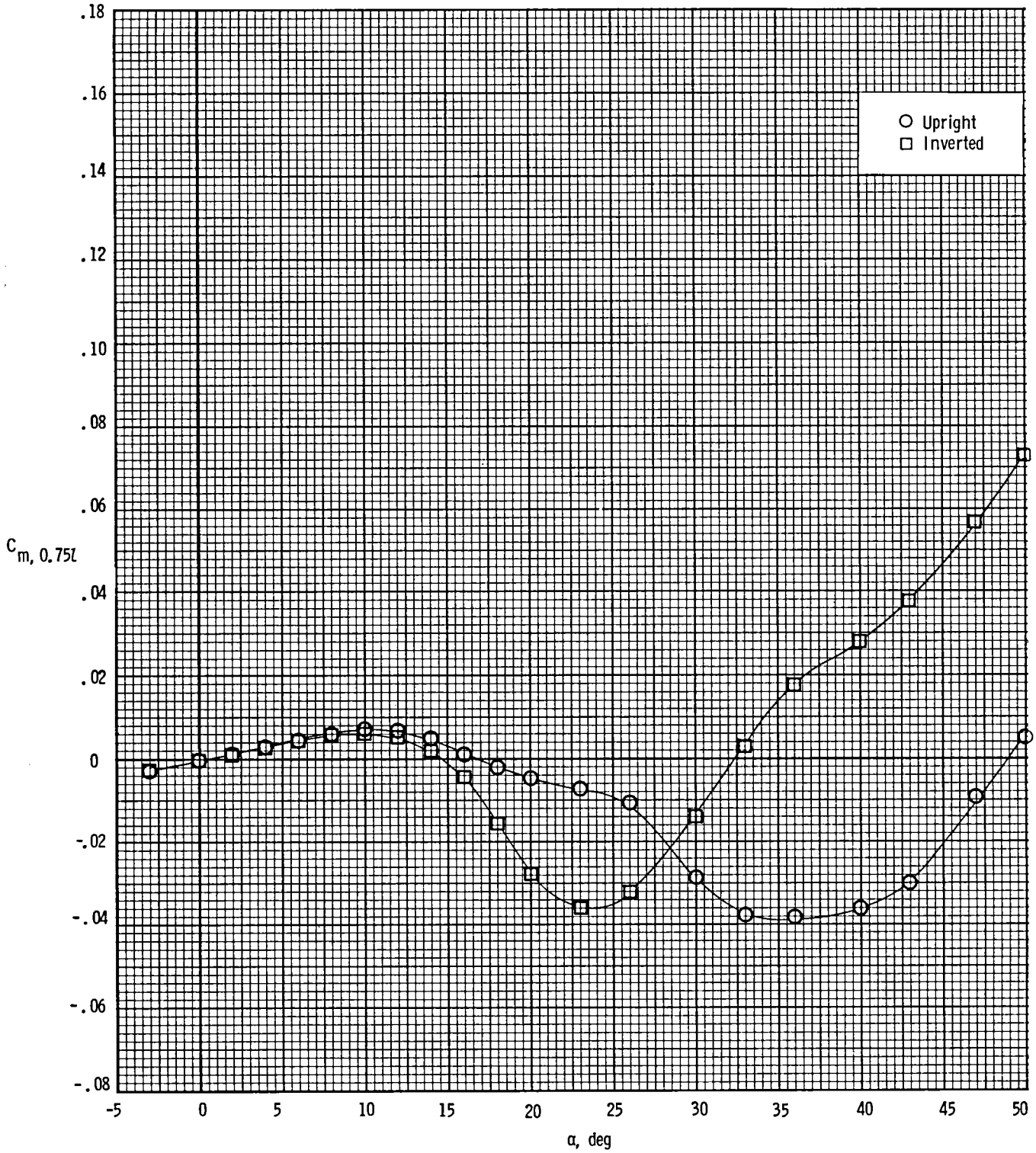

(d) $C_{m,0.75l}$ plotted against α.

Figure 3. Continued.

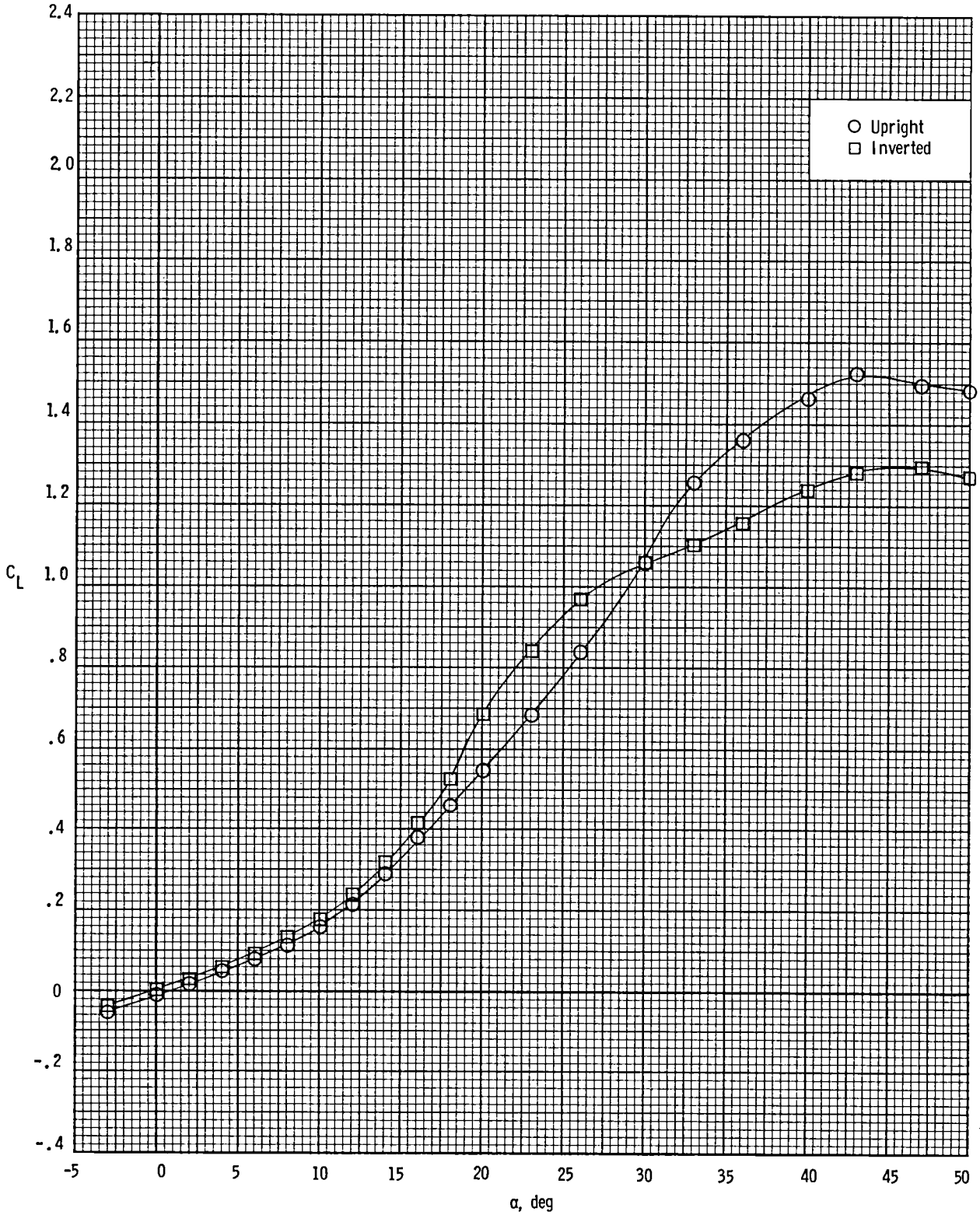

(e) C_L plotted against α.

Figure 3. Continued.

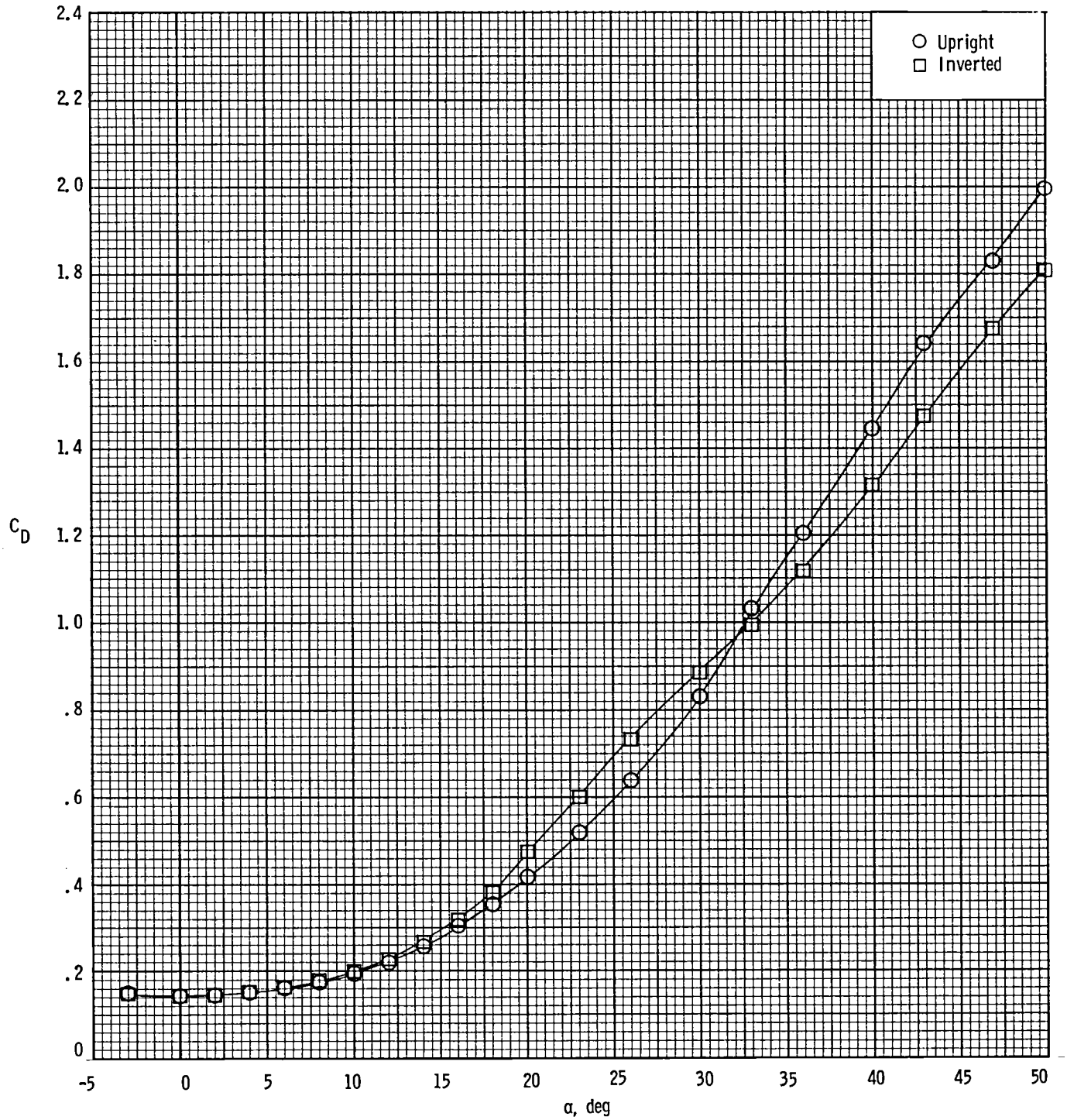

(f) C_D plotted against α.

Figure 3. Continued.

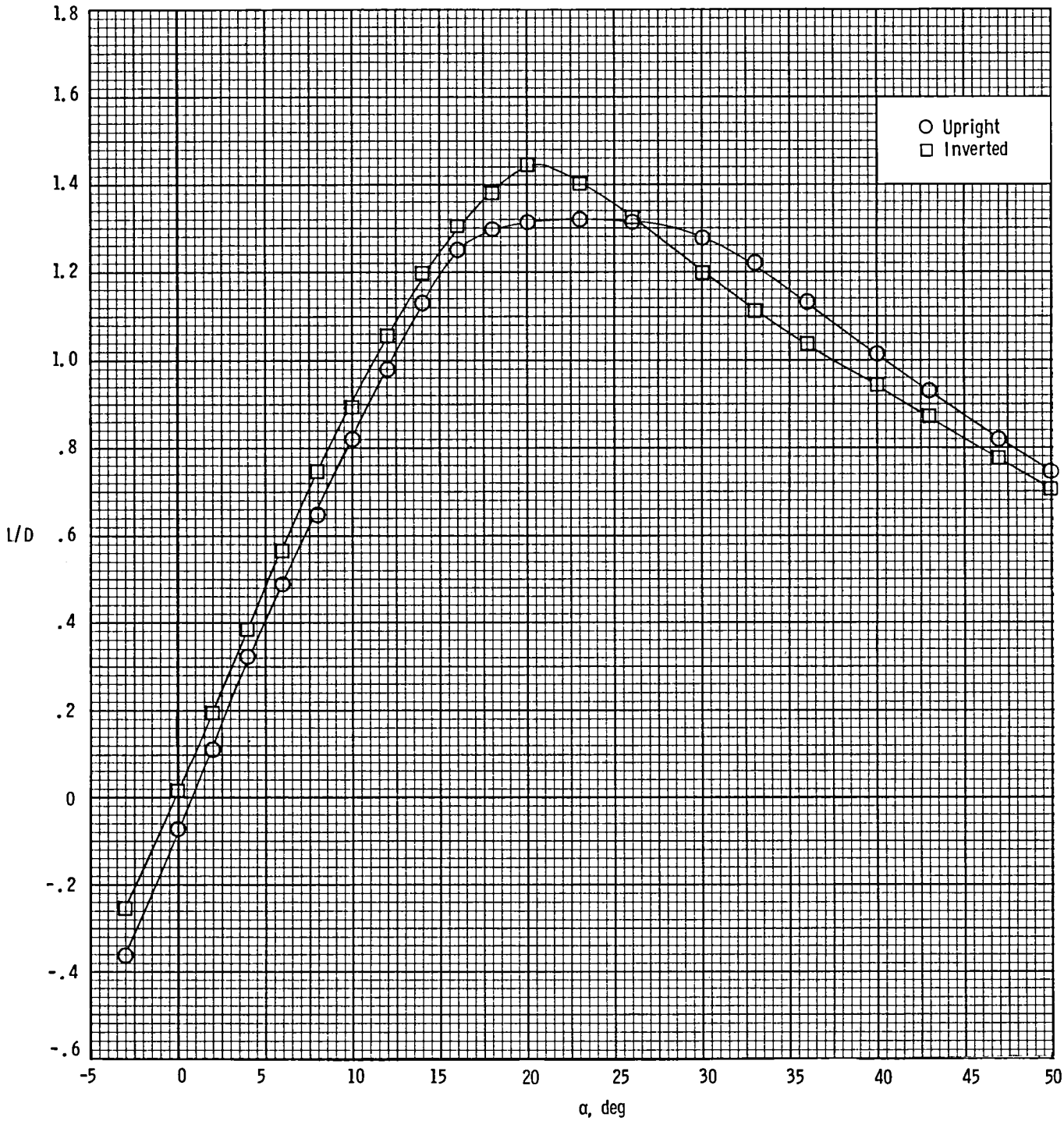

(g) L/D plotted against α.

Figure 3. Continued.

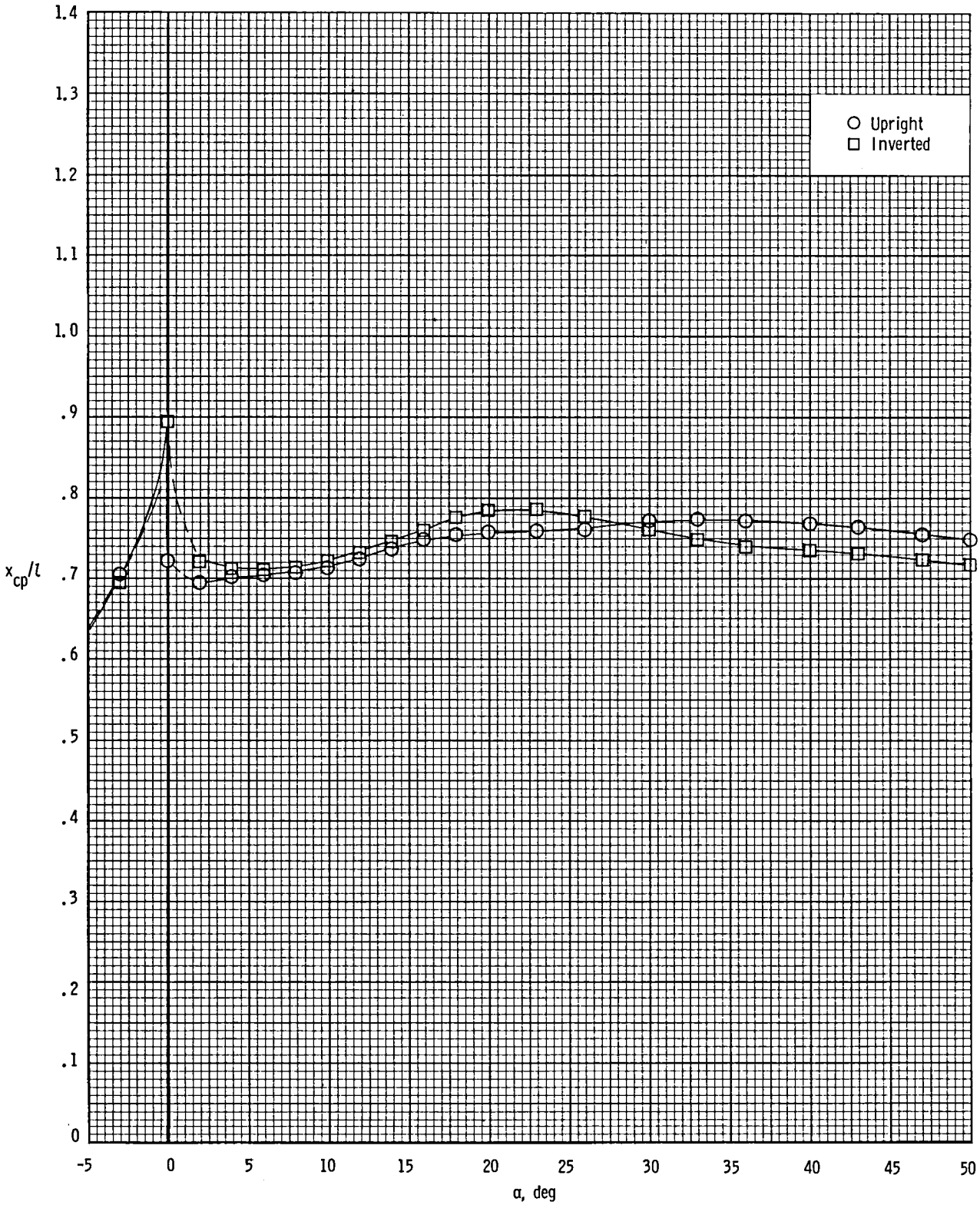

(h) x_{cp}/l plotted against α.

Figure 3. Concluded.

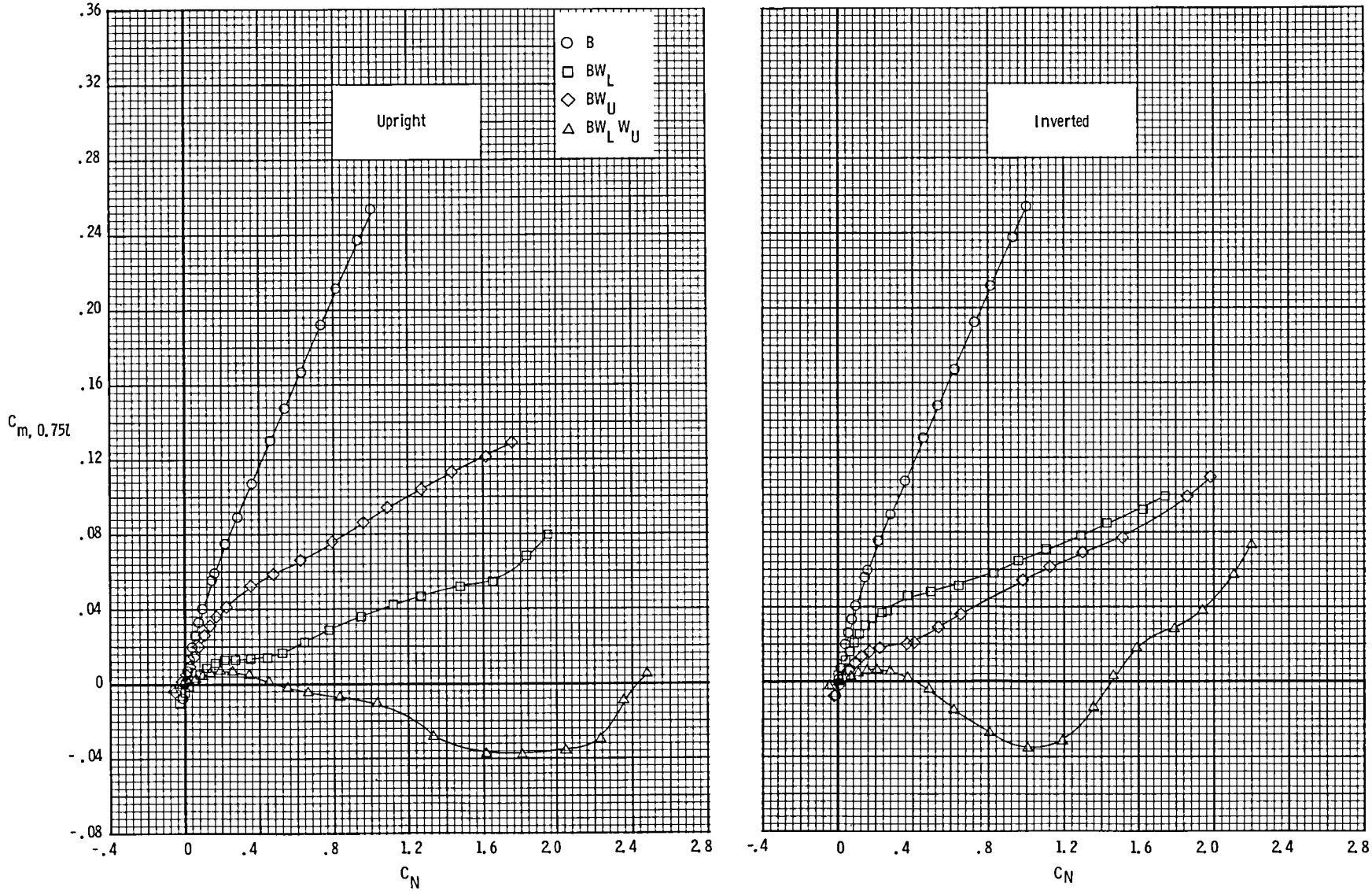

(a) $C_{m,0.75l}$ plotted against C_N.

Figure 4. Effects of component buildup on longitudinal characteristics for upright and inverted positions.

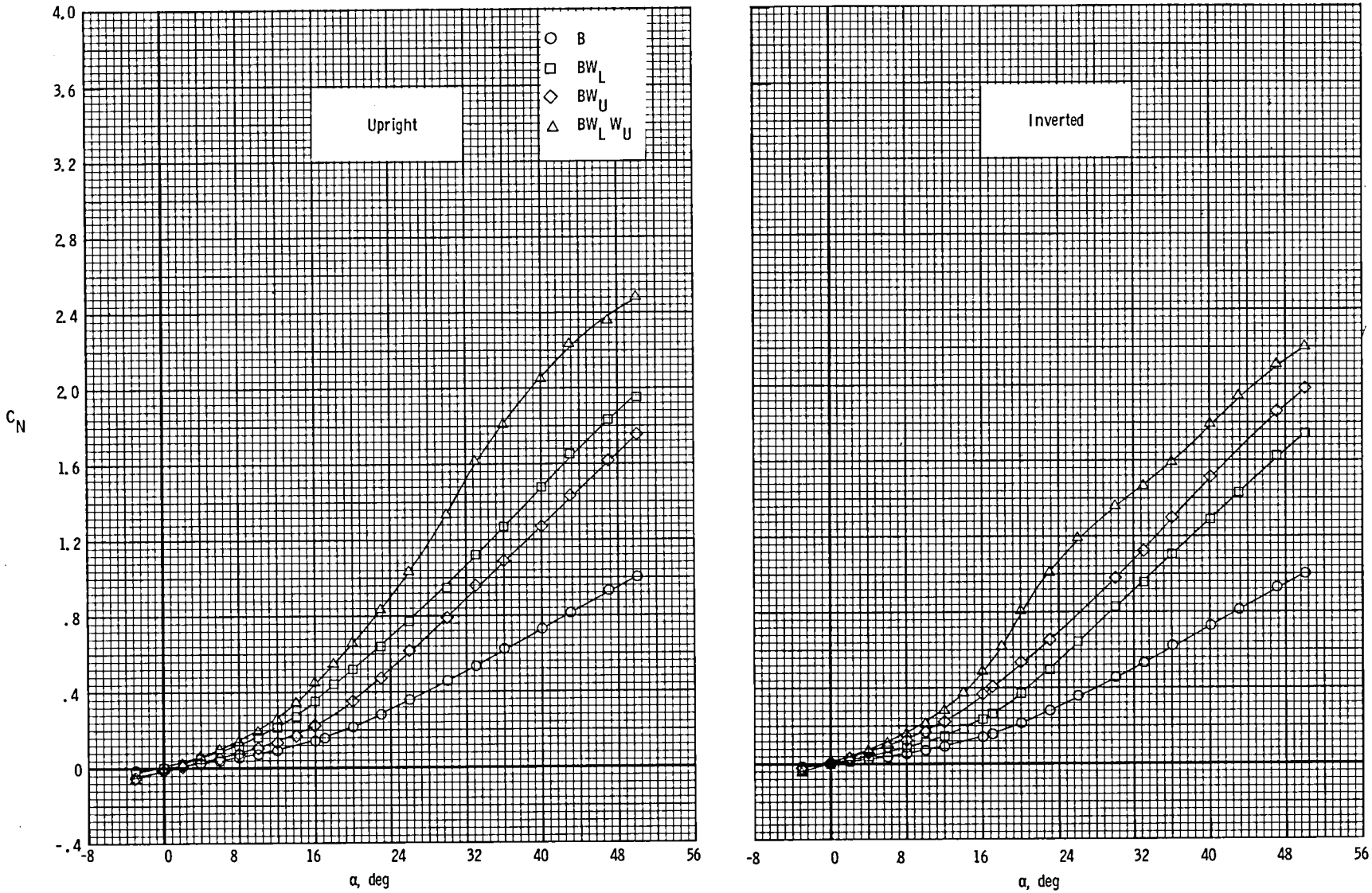

(b) C_N plotted against α.

Figure 4. Continued.

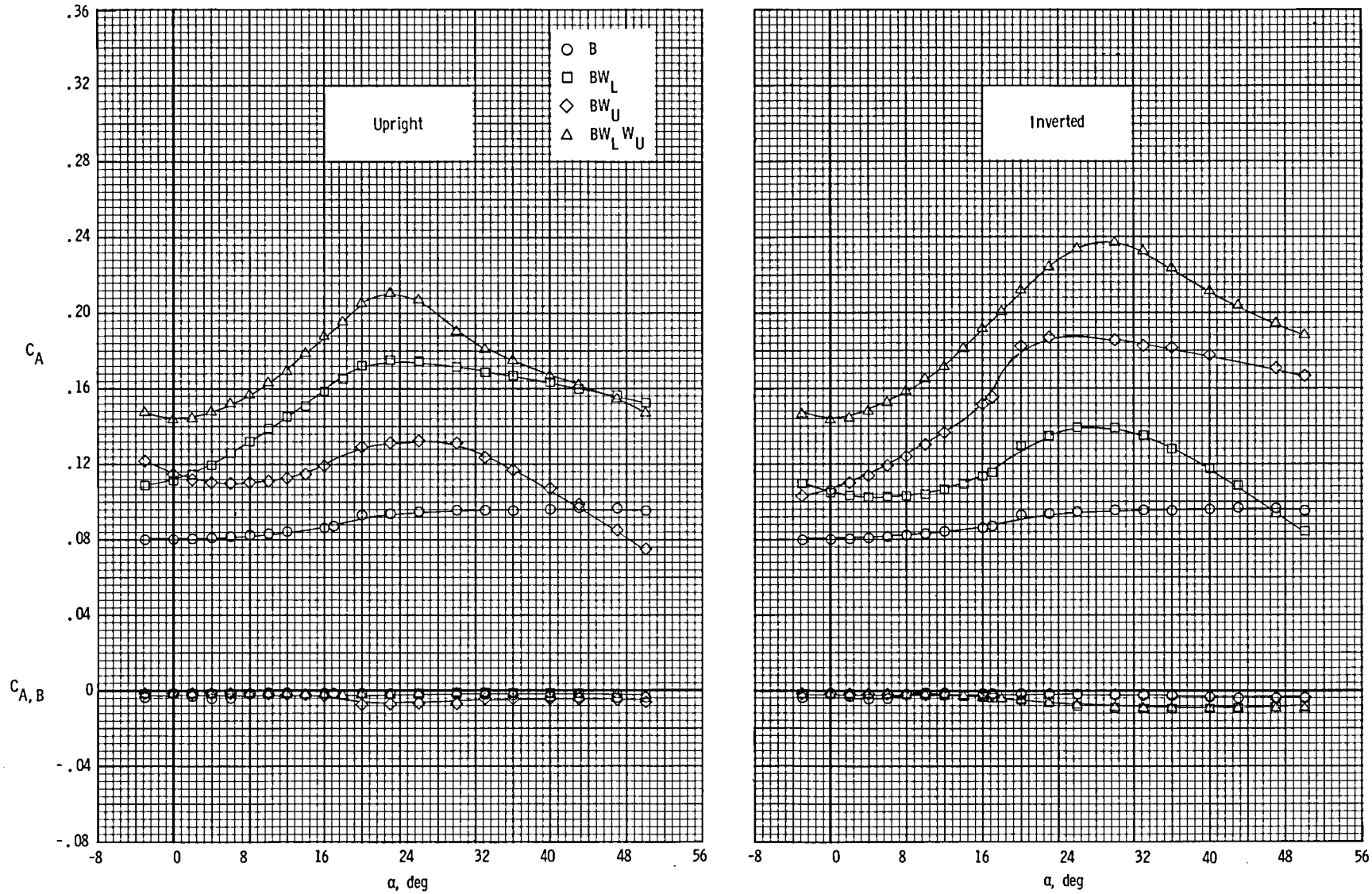

(c) C_A and $C_{A,B}$ plotted against α.

Figure 4. Continued.

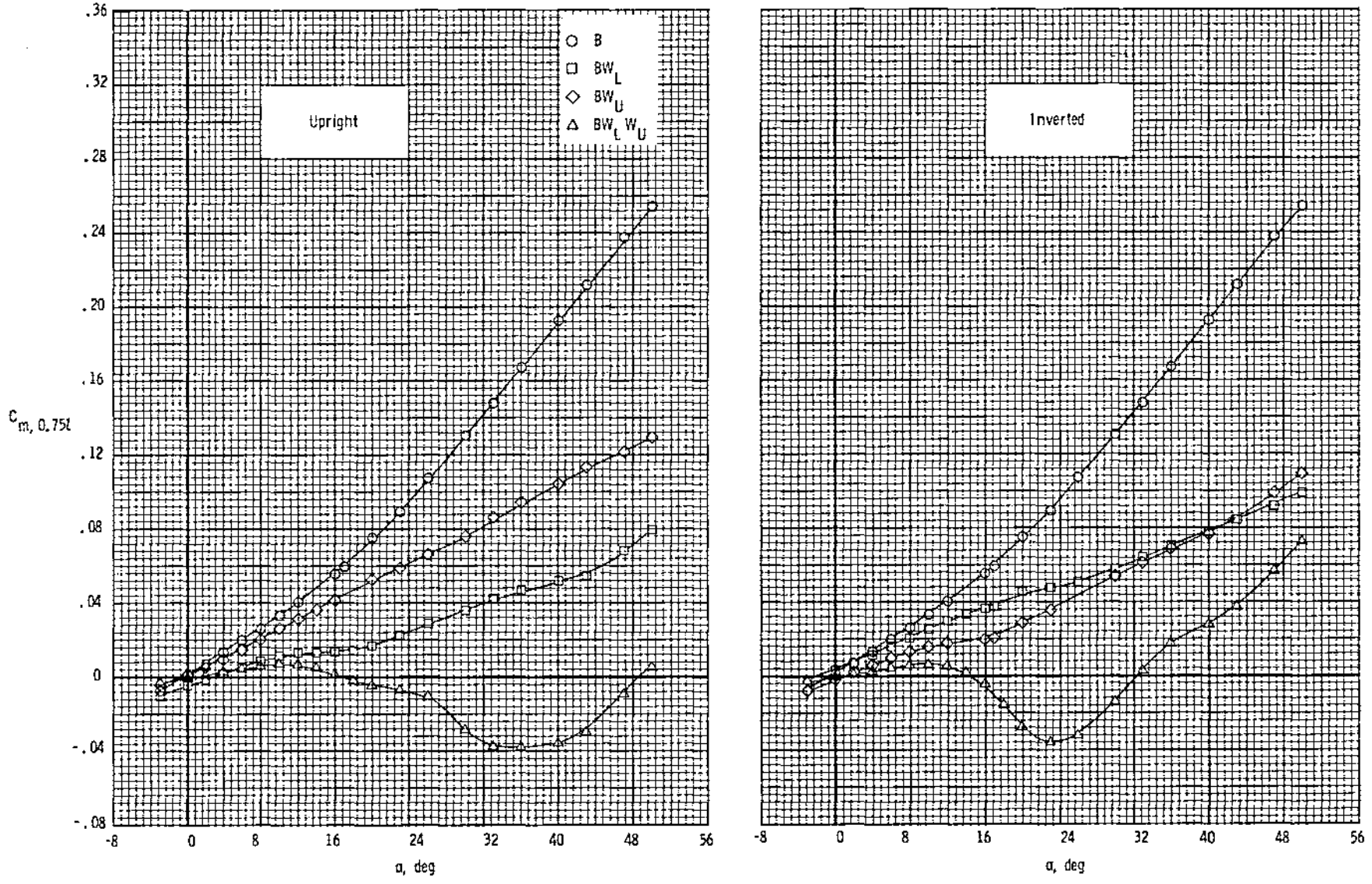

(d) $C_{m,0.75\ell}$ plotted against α.

Figure 4. Continued.

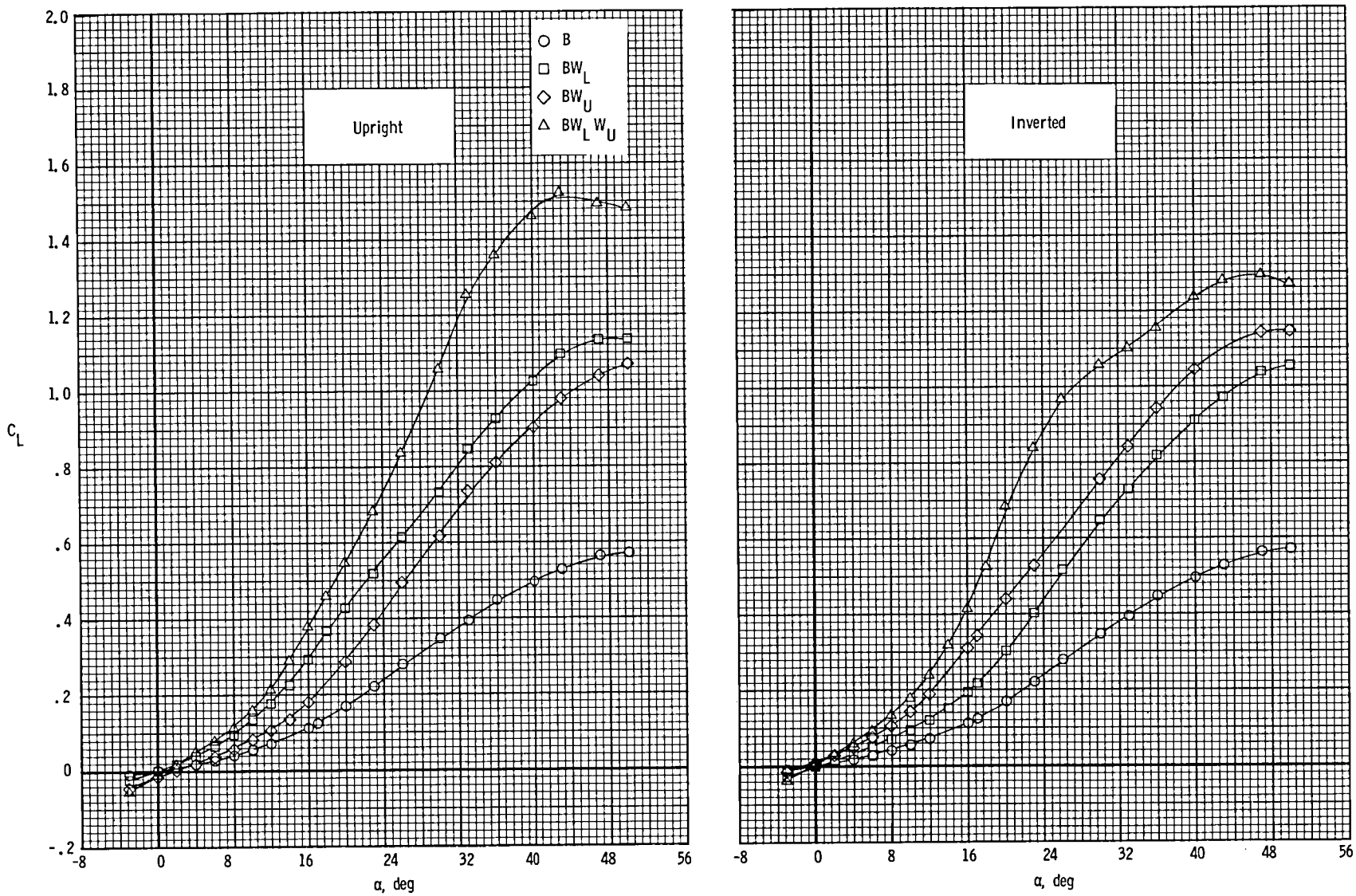

(e) C_L plotted against α.

Figure 4. Continued.

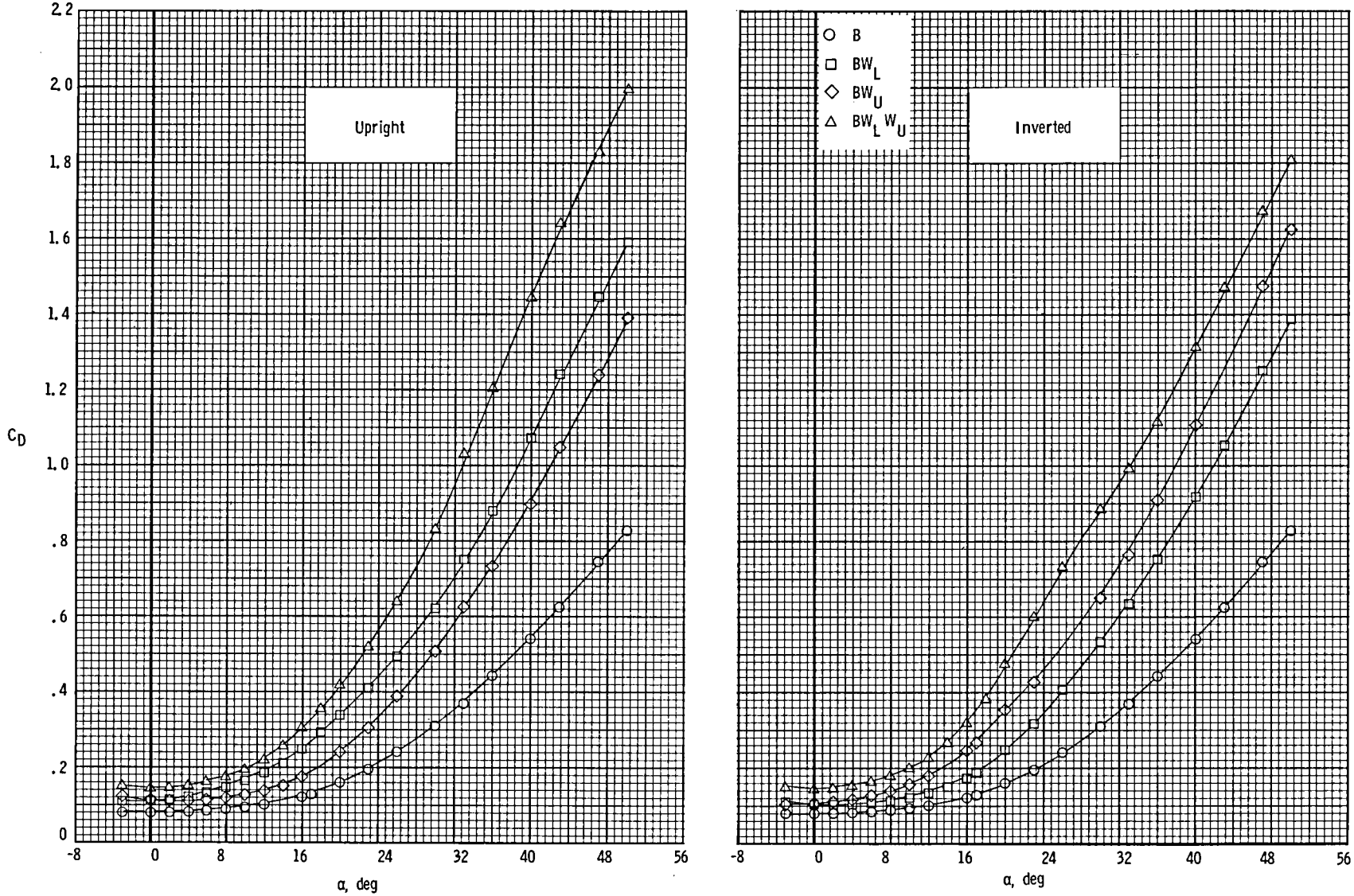

(f) C_D plotted against α.

Figure 4. Continued.

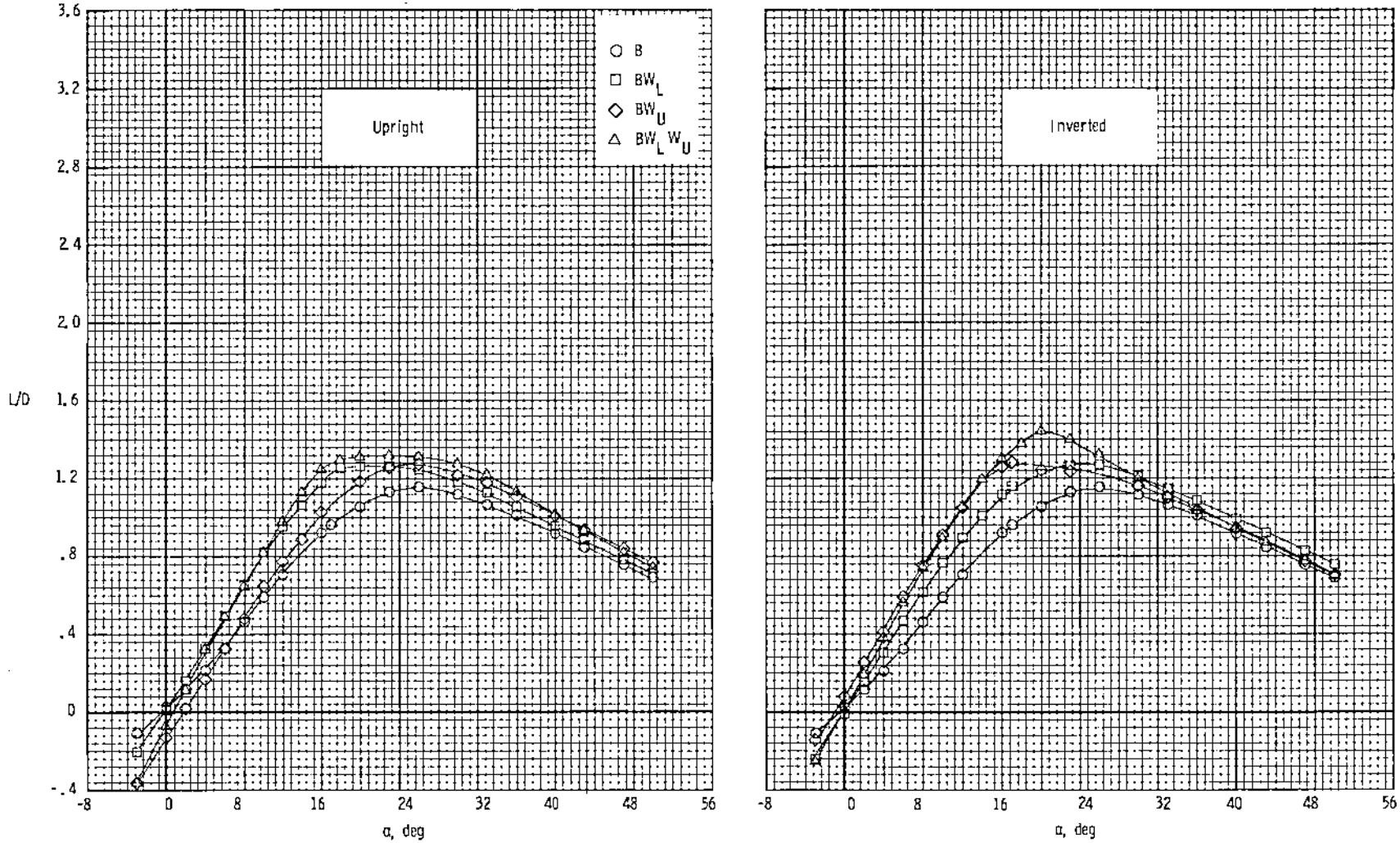

(g) L/D plotted against α.

Figure 4. Continued.

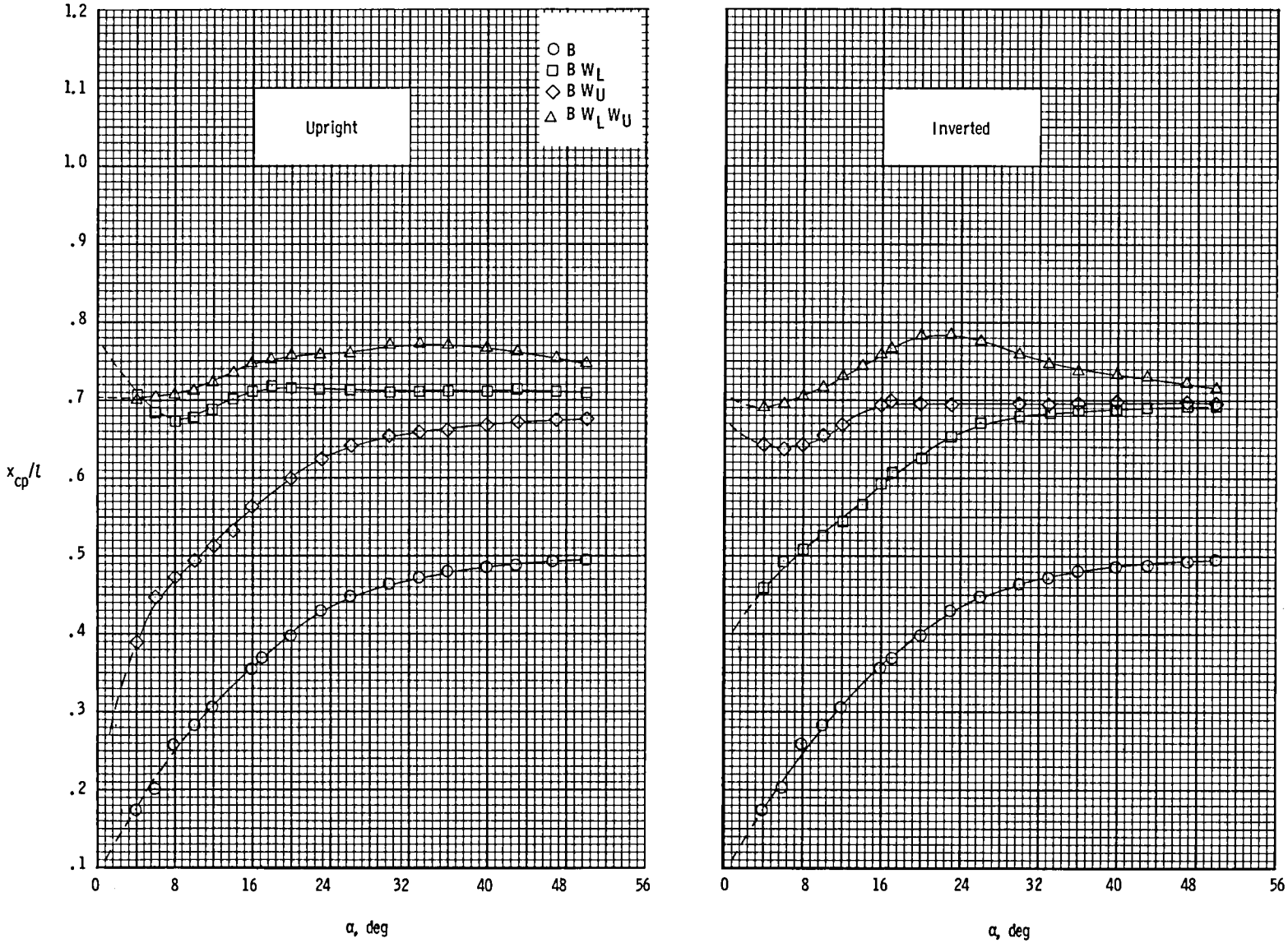

(h) x_{cp}/l plotted against α.

Figure 4. Concluded.

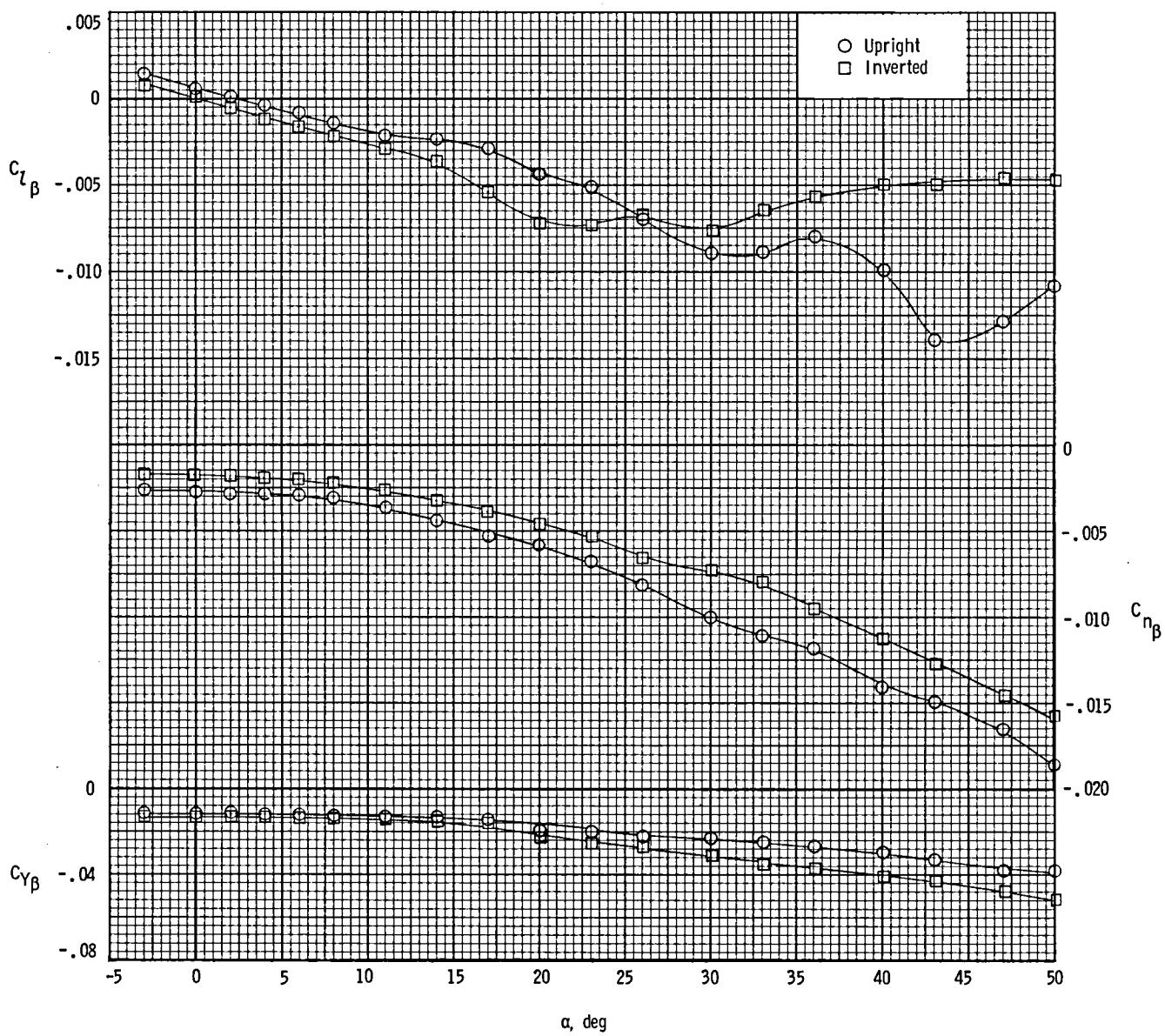

Figure 5. Lateral-directional characteristics of complete configuration in upright and inverted positions. $M = 20.3$; $R_l = 3.2 \times 10^6$.

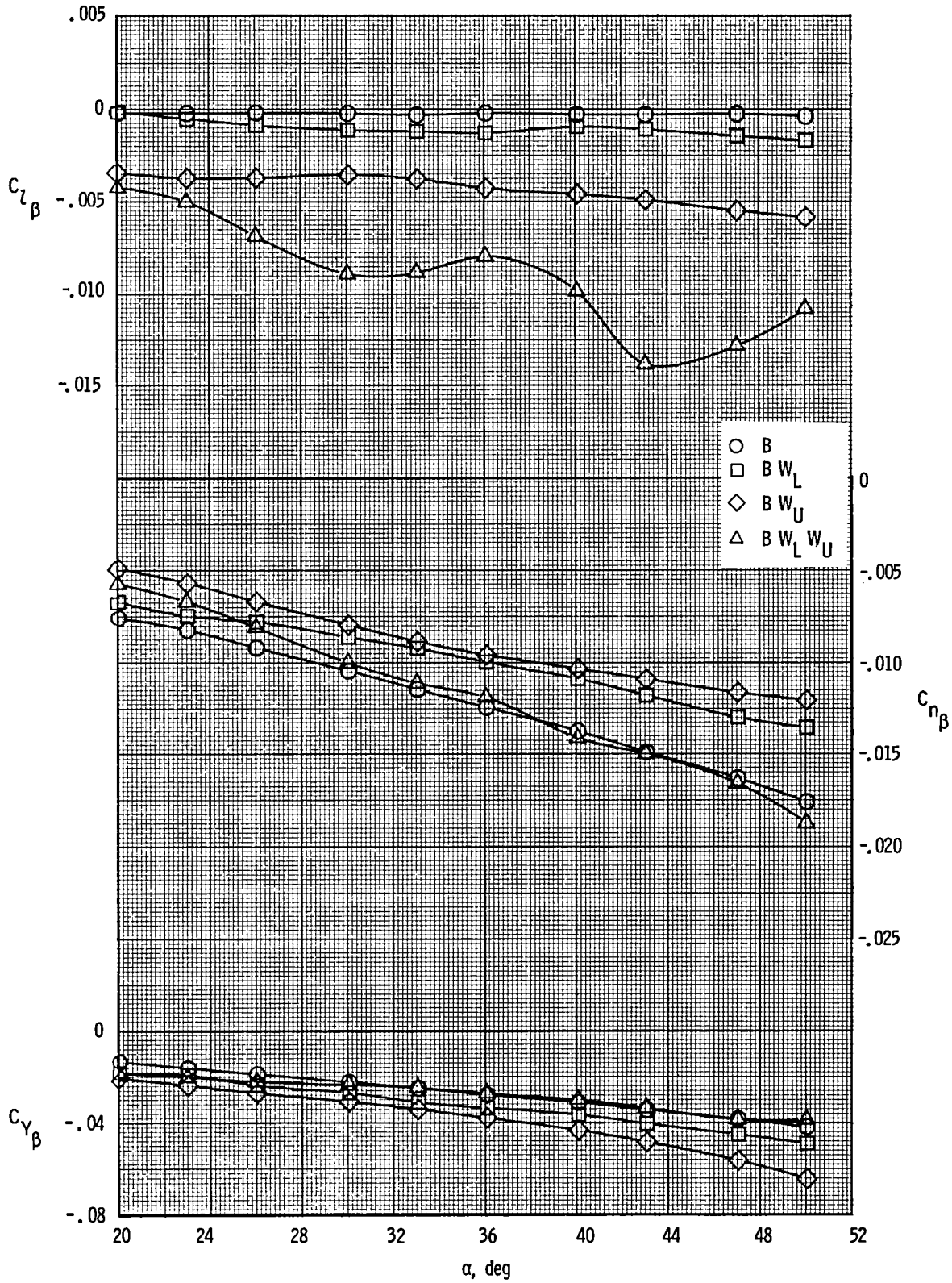

(a) Upright position.

Figure 6. Effect of component buildup on lateral-directional characteristics for upright and inverted positions.

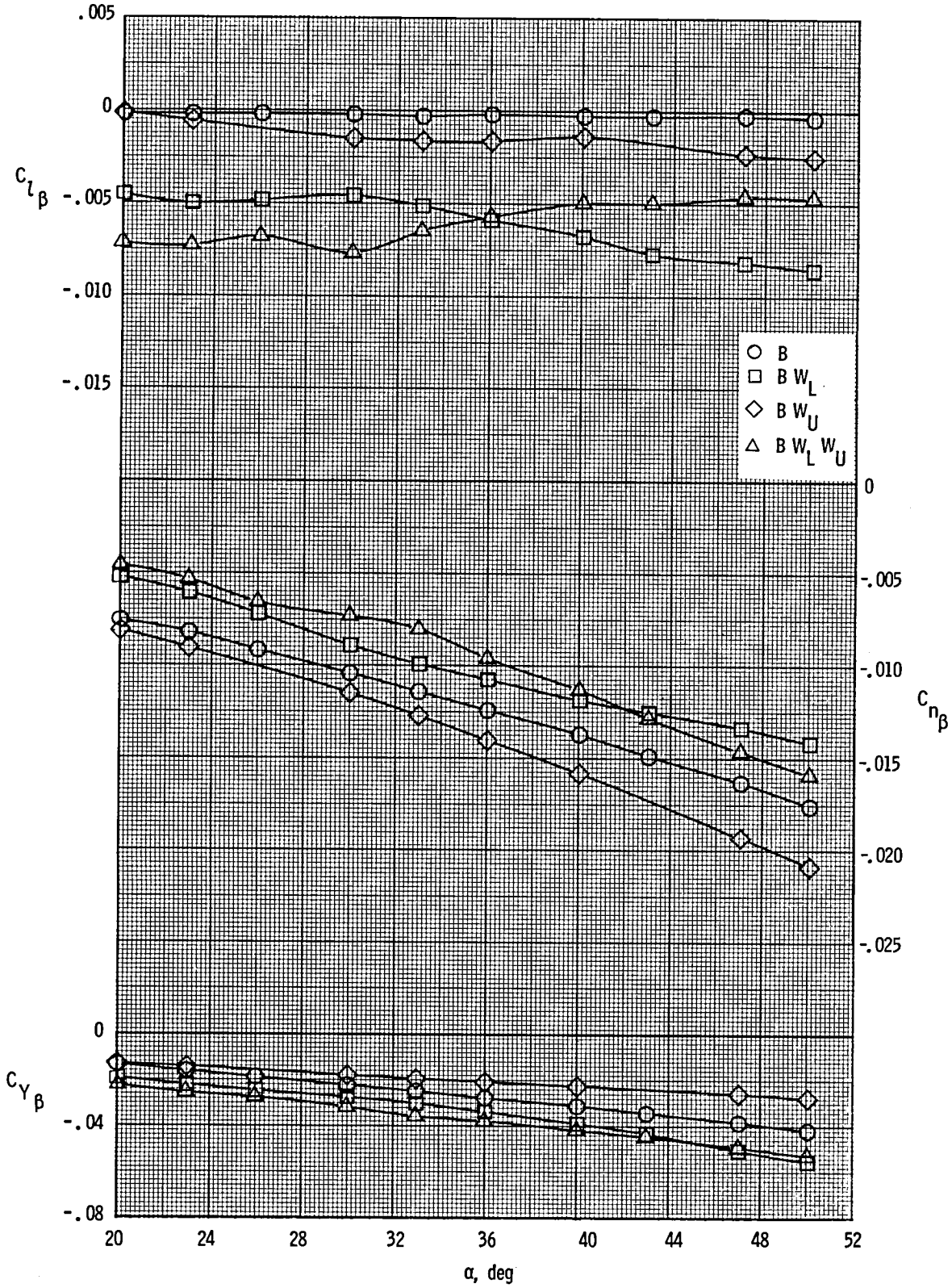

(b) Inverted position.

Figure 6. Concluded.

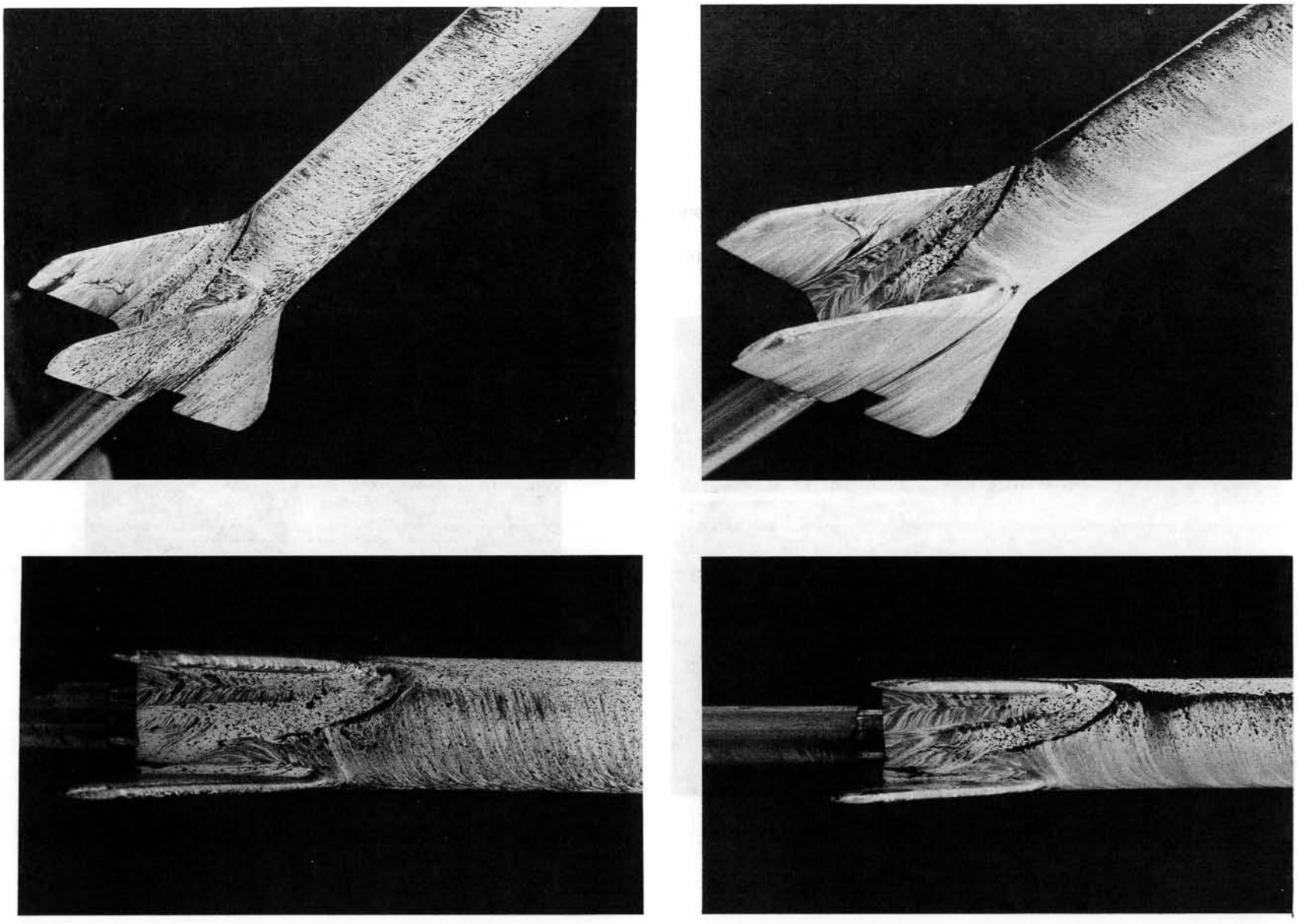

(a) $\alpha = 30°$.

(b) $\alpha = 40°$.

L-84-10,695

Figure 7. Oil-flow patterns on right side of upright model.

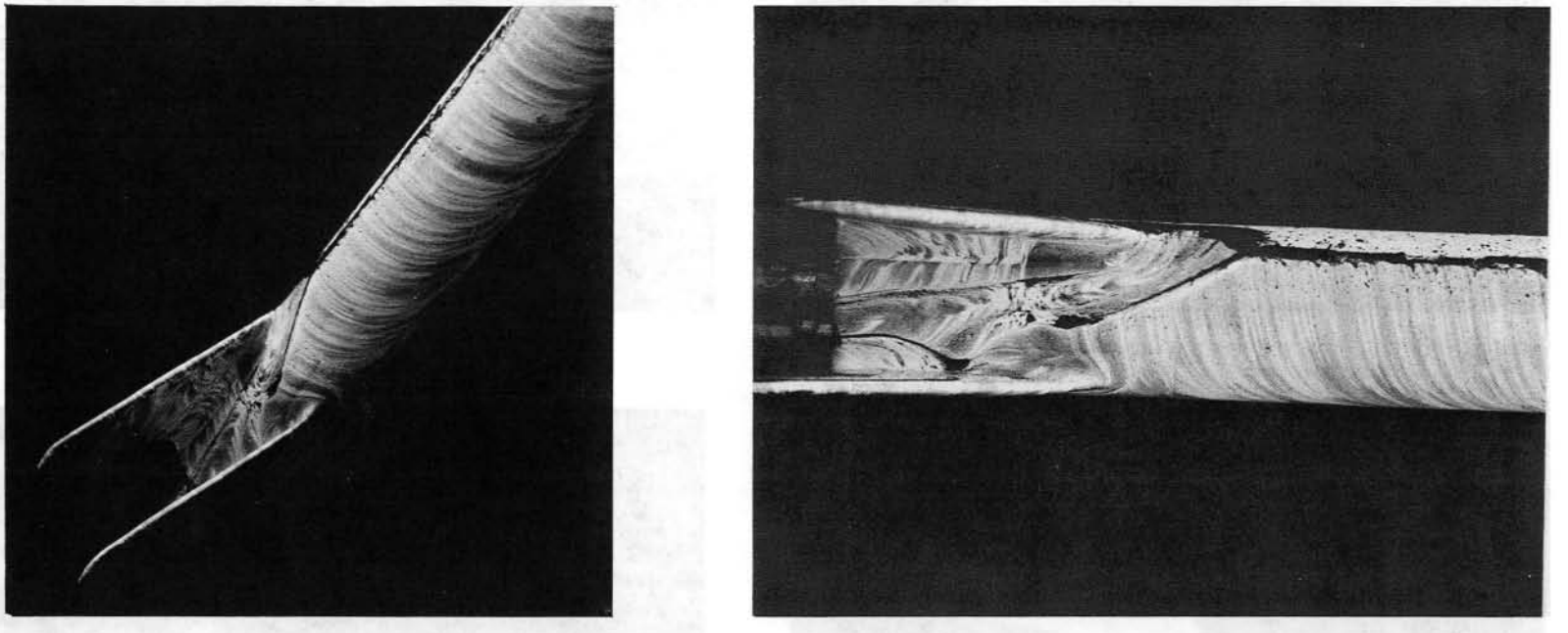

L-84-10,696

(c) $\alpha = 50°$.

Figure 7. Concluded.

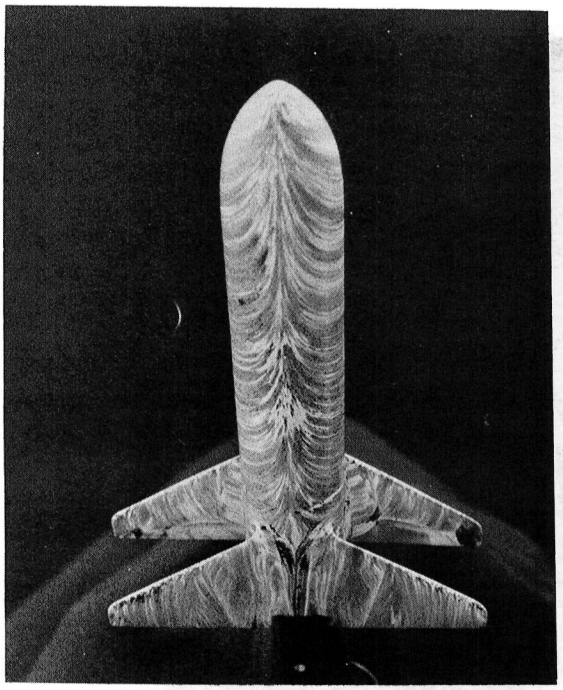

$\alpha = 30^{o}$

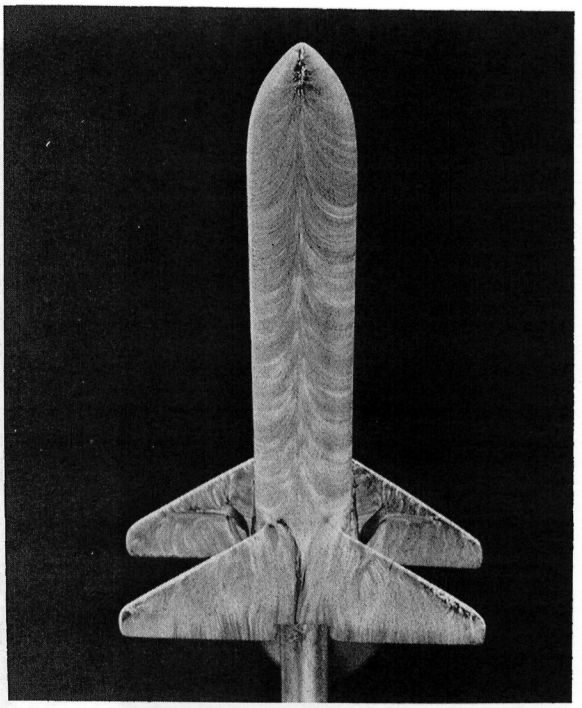

$\alpha = 40^{o}$

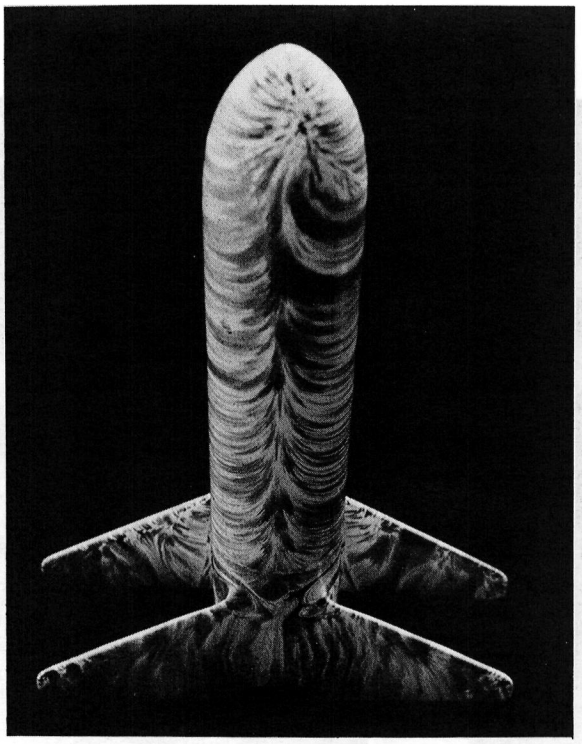

$\alpha = 50^{o}$

L-84-10,697

Figure 8. Oil-flow patterns on bottom surface of upright model.

$\alpha = 20^{o}$

$\alpha = 30^{o}$

$\alpha = 40^{o}$

$\alpha = 50^{o}$

L-84-10,698

Figure 9. Photographs of flow fields on complete model.

1. Report No.	2. Government Accession No.	3. Recipient's Catalog No.
NASA TM-86314		

4. Title and Subtitle	5. Report Date
EXPLORATORY INVESTIGATION OF THE AERODYNAMIC CHARACTERISTICS OF A BIWING VEHICLE AT MACH 20.3	February 1985
	6. Performing Organization Code: 506-51-13-02
7. Author(s): Peter T. Bernot	8. Performing Organization Report No.: L-15863
9. Performing Organization Name and Address: NASA Langley Research Center, Hampton, VA 23665	10. Work Unit No.
	11. Contract or Grant No.
12. Sponsoring Agency Name and Address: National Aeronautics and Space Administration, Washington, DC 20546	13. Type of Report and Period Covered: Technical Memorandum
	14. Sponsoring Agency Code

15. Supplementary Notes

16. Abstract

Longitudinal and lateral-directional characteristics of a simple biwing configuration were determined over an angle-of-attack range from −3° to 50°. The body was comprised of a cylindrical section with an ogival forebody having an overall fineness ratio of 6.67. The delta wings had a 38.3° sweep angle and were geometrically similar in planform. The upper wing was located slightly forward relative to the lower wing. The model was tested in upright and inverted orientations including component buildups. This investigation was conducted in the 22-inch aerodynamics leg of the Langley Hypersonic Helium Tunnel Facility.

17. Key Words (Suggested by Authors(s))	18. Distribution Statement
Advanced space transportation systems Entry vehicle aerodynamics	Unclassified—Unlimited Subject Category 18

19. Security Classif.(of this report)	20. Security Classif.(of this page)	21. No. of Pages	22. Price
Unclassified	Unclassified	31	A03

For sale by the National Technical Information Service, Springfield, Virginia 22161

NASA-Langley, 1985

National Aeronautics and
Space Administration

Washington, D.C.
20546

Official Business
Penalty for Private Use, $300

THIRD-CLASS BULK RATE

Postage and Fees Paid
National Aeronautics and
Space Administration
NASA-451

POSTMASTER: If Undeliverable (Section 158 Postal Manual) Do Not Return